SCIENCE CHINA
Information Sciences

• RESEARCH PAPER •

November 2024, Vol. 67, Iss. 11, 212203:1–212203:17
https://doi.org/10.1007/s11432-023-4109-6

Anti-asynchrony output regulation for switched systems under switching-Q-learning event-triggering against DoS attacks

Lili LI[1], Yalin CHEN[1], Dan MA[2,3*] & Qingjun GUO[1]

[1]*College of Marine Electrical Engineering, Dalian Maritime University, Dalian* 116026*, China;*
[2]*State Key Laboratory of Synthetical Automation for Process Industries, Northeastern University, Shenyang* 110819*, China;*
[3]*College of Information Science and Engineering, Northeastern University, Shenyang* 110819*, China*

Received 13 December 2023/Revised 6 February 2024/Accepted 21 March 2024/Published online 15 October 2024

Abstract This paper proposes a secure output regulation (SOR) scheme for network switched systems (NSSs) experiencing severely unstable dynamics (SUDs). This scheme aims to address the complex consecutive asynchrony caused by long-duration denial-of-service (LDDoS) attacks. When the denial-of-service (DoS) attack lasts longer than the dwell time of each subsystem, switching to a new subsystem is necessary to manage the unstable dynamic behavior caused by SUDs. The controller cannot immediately obtain information about the new modality. However, owing to the delayed access to new modality information by the controller, consecutive asynchrony occurs. To tackle this, we propose a resilient switching rule that mitigates the impact of consecutive asynchrony by choosing the optimal subsystem once the minimum dwell time is met. Multi-stage event-triggering mechanisms (METMs) are proposed to coordinate with switching signals by incorporating modality matching conditions and a switching-Q-learning algorithm. These mechanisms reduce asynchronous durations by aligning modality matching conditions and terminating attacks using attack parameters. This control scheme for SOR of NSSs with SUDs disturbed by LDDoS attacks provides a detailed analysis of dynamic switching behavior, leveraging the resilient switching rule and METMs. Finally, the feasibility of the proposed methodology is substantiated through simulations with an F-18 aircraft model.

Keywords switched systems, long-duration DoS attacks, consecutive asynchrony, switching-Q-learning algorithm, multi-stage event-triggering, resilient switching rule

1 Introduction

With the rapid development of industries, large-scale multi-model control systems with hybrid characteristics have proliferated. Examples include switching models for underwater vehicles, autonomous vehicles, and intelligent vehicles [1–3]. These types of systems are best modeled as networked switched systems (NSSs), where a shared network facilitates communication between the individual control components. However, data transmission in NSSs is vulnerable to both network-induced issues and cyber attacks. A particularly destructive type of cyber attack is the denial-of-service (DoS) attack, which destabilizes systems by blocking communication networks and preventing remote controllers and actuators from receiving the transmitted system outputs, control inputs, and switching signals. Aperiodic DoS attacks, which have restricted frequency and duration, are more realistic since they require less prior knowledge of the systems. Previous studies [4, 5] have explored aperiodic DoS attacks on NSSs, considering the asynchronous switching behavior of these systems. In some cases, the duration of DoS attacks remains within the dwell time (DT) of the activated subsystem [4], or attacks are initiated at switching instants [5]. Several switching rules were designed to handle the challenges posed by aperiodic DoS attacks that extend over several consecutive activation intervals [6–8]. For NSSs with partially unstable subsystems and all unstable switching instants, the mode-dependent average DT (MDADT) switching rule in [6] was introduced. This rule imposes constraints on the lower bound of MDADT for stable and unstable subsystems and limits the average time proportion of unstable subsystems. Similarly, the average DT

* Corresponding author (email: madan@mail.neu.edu.cn)

(ADT) switching rule in [7] sets restrictions on the lower bound of the ADT for subsystems associated with the frequency and duration of DoS attacks. For NSS with severely unstable dynamics (SUDs), where all unstable subsystems are unstable and some switching moments are unstable, the DT switching rule in [8] restricts the activation interval of unstable subsystems by adding the maximum DT containing the DoS attack parameter and by imposing limits on the stable-to-unstable switching ratio. In general, these flexible switching rules [6–8] address consecutive asynchronous switching without specifying particular switching instants and target subsystems. This ambiguity leads to redundant and long-lasting consecutive asynchronous switching dynamics between subsystems and sub-controllers, posing significant challenges to maintaining system stability.

Given the multi-modal characteristic of switched systems, the choice of modality by the switching rules is crucial for ensuring system stability, regardless of whether it is stable or not. Initially, research on time-dependent switching focused on scenarios where all subsystems were stable [9]. This research evolved to address cases with partially unstable subsystems [10] to fully unstable subsystems [11], and even SUDs [12]. However, slow switching, which requires subsystems to dwell for a period, is unsuitable for cases involving fast modality changes, where the activated modalities are ambiguous. To address this, state-dependent switching rules that guarantee fast switching were proposed in [13], allowing adjacent Lyapunov functions to jump at the switching instant [14, 15]. However, excessively fast switching may cause chattering in physical devices. To integrate the benefits of slow and fast switching, state-dependent switching rules adhering to a DT constraint were developed, such as [16–18]. A hybrid switching rule for synchronous switching with all switching instants was presented in [16]. These hybrid rules also permitted asynchronous switching, allowing for upward or downward jumps in the Lyapunov function at switching instants of subsystems and controllers [17, 18]. These hybrid switching rules are valuable for selecting the appropriate switching instants and target subsystems by state-dependent switching conditions after a period of dwelling. Consequently, they effectively address redundant asynchronous switching induced by long-lasting DoS attacks.

Owing to the widespread adoption of network technologies, event-triggered mechanisms (ETMs) have been suggested to better manage communication resources [19], leading to the development of numerous beneficial ETMs. Most current ETMs aim to enhance control performance by formulating error detection conditions using system information, which, in turn, helps adjust the data update interval. These thresholds in error detection conditions can be static [20–22], adaptive [23, 24], or even adjustable according to intelligent optimization algorithms [25, 26]. In particular, Q-learning and A3C algorithms in [25, 26] were utilized to optimize trigger thresholds by learning value functions from system outputs and trigger thresholds. Furthermore, deep Q-networks were used in [27] to learn event-triggering strategies. Multiple event-triggering conditions can also be explored to associate with error detection conditions in ETMs for better coordination of data transmission against switching [8, 12, 28] and cyber attacks [7, 8, 26, 29]. In [7,8,26,29], acknowledgment character (ACK) techniques have been introduced to monitor and update the data transmission interval blocked by DoS attacks. In [8, 12, 28], to reduce asynchronous durations after subsystem switching, a modality-matching condition has been added to ETMs. Inspired by these discussions, an important topic for further exploration is how to reasonably utilize intelligent algorithms and schedule multiple event-triggering conditions in ETMs. This approach could reduce consecutive asynchronous durations caused by DoS attacks and switching.

This paper proposes a secure output regulation (SOR) scheme tailored for NSSs with SUDs under long-duration denial-of-service (LDDoS) attacks. The main contributions are summarized as follows. (1) The presented resilient switching rule flexibly selects the target subsystem and appropriate switching instant to mitigate asynchronous switching. In situations where LDDoS attacks are absent, the target subsystem that satisfies the resilient switching condition is selected after a minimum DT. When an LDDoS attack occurs, the target subsystem is selected at the maximum DT, incorporating an indefinite matrix to account for unstable switching instants. Importantly, the stability of subsystem switching is independent of the stability of the corresponding controller switching. (2) Multi-stage event-triggered mechanisms (METMs) are developed to coordinate with switching signals and attack parameters. During the error detection stage, a switching-Q-learning algorithm is proposed to determine the optimal triggering threshold via two phases. Initially, the Q-learning algorithm is employed to compute some candidate triggering thresholds for all subsystems. Subsequently, for subsystems in operation, the optimal threshold is selected from the previous candidate thresholds based on the switching signals of the subsystem and sub-controller. The modality matching stage and the attack-based stage were introduced into METMs that shorten the asynchronous duration by adding specific triggering instances. (3) The proposed SOR scheme integrates

METMs, resilient switching rules, and dynamic output feedback controllers (DOFCs). This integration effectively mitigates consecutive asynchronous switching by addressing five possible scenarios associated with dynamic switching behavior based on the relationship between attack durations and dwell-time durations. The paper also provides solvability conditions for the SOR problem.

2 Problem formulation

2.1 System model and DOFC

The considered NSSs with SUDs are described as

$$\begin{cases} \dot{x}(t) = A_\sigma x(t) + B_\sigma u(t) + D_\sigma \omega(t), \\ y(t) = C_\sigma x(t) + E_\sigma \omega(t), \\ \dot{\omega}(t) = G_\sigma \omega(t), \end{cases} \tag{1}$$

where $x(t) \in \mathbb{R}^{n_x}$, $u(t) \in \mathbb{R}^{n_u}$, $y(t) \in \mathbb{R}^{n_y}$, and $\omega(t) \in \mathbb{R}^{n_\omega}$ are state, control input, regulated output, and exogenous input, respectively. A_σ, B_σ, C_σ, D_{σ_p}, E_σ, and G_σ are given constant matrices with suitable dimensions. All eigenvalues of G_σ possess non-negative real components. $\sigma = \sigma(t) : [0, \infty) \to \mathbb{L} = \{1, 2, \ldots, \bar{l}\}$ is the switching signal, where $\bar{l}$ is the subsystems number. And the switching sequence corresponding to σ is defined as $\mathcal{L}_s = \{\ell_q\}_{q=1}^{N_\sigma(0,t)}$ with $\ell_0 = 0$. $N_\sigma(0,t)$ is the subsystem switching number on $[0,t)$. The mentioned SUDs specifically encompass the unsolvable OR for individual subsystems and some unstable switchings. This refers specifically to the scenario where the Lyapunov function fails to monotonically decrease over each activation interval and some switching instants.

The DOFC is governed as

$$\begin{cases} \dot{x}_c(t) = F_\phi x_c(t) + L_\phi x_c(gh) + H_\phi \hat{y}(t), \\ \hat{u}(t) = K_\phi x_c(t), \end{cases} \tag{2}$$

where $x_c \in \mathbb{R}^{n_{x_c}}$, $\hat{y} \in \mathbb{R}^{n_y}$, $\hat{u} \in \mathbb{R}^{n_u}$, and $\phi = \phi(t) \in \mathbb{L}$ are state vector, input, output, and switching signal of the controller. gh is the sampling instant, F_ϕ, L_ϕ, H_ϕ, K_ϕ are the desired matrices with appropriate dimensions. The sub-controller switching has the stable sequence $\mathcal{L}_c^- = \{\tilde{\ell}_{q_3}^-\}_{q_3=1}^{n_c^-}$ and the unstable sequence $\mathcal{L}_c^+ = \{\tilde{\ell}_{q_4}^+\}_{q_4=1}^{n_c^+}$.

2.2 Dual networks and LDDoS attacks

The dual networks between the system and the controller may suffer from transmission delays and LDDoS attacks in both the sampler-to-controller (S2C) and controller-to-actuator (C2A) channels. The transmission delay τ_r^ς of the r-th triggering instant satisfies $\tau_m^\varsigma \leqslant \tau_r^\varsigma \leqslant \tau_M^\varsigma \leqslant h$ with $r \in \mathbb{N}^+$, $\varsigma \in \{y, \hat{u}\}$, $\tau_m^\varsigma = \min_{r\in\mathbb{N}^+}\{\tau_r^\varsigma\}$, and $\tau_M^\varsigma = \max_{r\in\mathbb{N}^+}\{\tau_r^\varsigma\}$. In dual networks, the activated instant of the p-th LDDoS attack is defined as h_p^ς, $p \in \mathbb{N}^+$, $\varsigma \in \{y, \hat{u}\}$. The corresponding attack interval is expressed as $\mathbb{H}_p^\varsigma = [h_p^\varsigma, h_p^\varsigma + d_p^\varsigma)$ with a duration $d_p^\varsigma > 0$. Further, the frequency and duration assumptions stated below impose restrictions on LDDoS attacks.

Assumption 1 (LDDoS attacks frequency [8])**.** There exist $w_d \geqslant 0$ and $\tau_d \geqslant h$ such that $N_d(\underline{t}, \overline{t}) \leqslant w_d + \frac{\overline{t}-\underline{t}}{\tau_d}$, where $N_d(\underline{t}, \overline{t})$ is the number of LDDoS attacks that transpire within the interval $[\underline{t}, \overline{t})$.

Assumption 2 (LDDoS attacks duration [8])**.** An upper bound $d_{\max} = \sup_{p\in\mathbb{N}^+}\{d_p^\varsigma\}$ and the lower bound $s_{\min} = \inf_{p\in\mathbb{N}^+}\{h_{p+1}^\varsigma - h_p^\varsigma - d_p^\varsigma\}$ exist for the activated intervals and sleeping intervals of DoS attacks such that $s_{\min} \geqslant h + \max\{\tau_m^y, \tau_m^{\hat{u}}\}$, $\mathcal{T}_{\max} < d_{\max} < \frac{(\bar{t}-\underline{t})}{N_d(\underline{t},\bar{t})}$, where $\mathcal{T}_{\max}$ is the maximum DT of the subsystems.

2.3 METMs

The METMs are designed with three stages involving attack parameters, the error detection condition, and the modality matching condition that enable the adjustment of data transmission in networks for NSSs (1).

The description of the METMs is presented as

$$t^{\varsigma}_{r+1}h = \min\{\bar{t}^{\varsigma}_{r+1}h,\ \hat{t}^{\varsigma}_{r+1}h,\ \tilde{t}^{\varsigma}_{r+1}h\}, \tag{3}$$

where

$$\bar{t}^{\varsigma}_{r+1}h = \min_{m\in\mathbb{N}}\{g^{\varsigma}_{r,m}h | g^{\varsigma}_{r,m}h = \hbar^{\varsigma}_{p},\ p\in\mathbb{N}^{+}\}, \tag{4}$$

$$\hat{t}^{\varsigma}_{r+1}h = \min_{m\in\mathbb{N}}\{g^{\varsigma}_{r,m}h | \Xi^{\varsigma}(g^{\varsigma}_{r,m}h) > 0\}, \tag{5}$$

$$\tilde{t}^{\varsigma}_{r+1}h = \min_{m\in\mathbb{N}}\{g^{\varsigma}_{r,m}h | o(g^{\varsigma}_{r,m}h) \neq o(g^{\varsigma}_{r,m}h - h)\}, \tag{6}$$

with $(\varsigma, o)\in\{(y,\sigma),(\hat{u},\phi)\}$, the first sampling instant $\hbar^{\varsigma}_{p}$ after $\mathbb{H}^{\varsigma}_{p}$, $p\in\mathbb{N}^{+}$, the m-th sampling instant $g^{\varsigma}_{r,m}h = t^{\varsigma}_{r}h + mh \notin \mathbb{H}^{\varsigma}_{p}$ after the triggering instant $t^{\varsigma}_{r}h$, and the error $\mathrm{e}^{\varsigma}(g^{\varsigma}_{r,m}h) = \varsigma(g^{\varsigma}_{r,m}h) - \varsigma(t^{\varsigma}_{r}h)$, $\Xi^{\varsigma}(g^{\varsigma}_{r,m}h) = \mathrm{e}^{\varsigma\mathrm{T}}(g^{\varsigma}_{r,m}h)\Omega^{\varsigma,1}_{o(t^{\varsigma}_{r}h)}\mathrm{e}^{\varsigma}(g^{\varsigma}_{r,m}h) - \delta^{\varsigma}_{\bar{o}(g^{\varsigma}_{r,m}h),\epsilon}\varsigma^{\mathrm{T}}(t^{\varsigma}_{r}h)\Omega^{\varsigma,2}_{o(t^{\varsigma}_{r}h)}\varsigma(t^{\varsigma}_{r}h)$. And $\delta^{\varsigma}_{\bar{o}(g^{\varsigma}_{r,m}h),\epsilon} = \delta^{\varsigma}_{\bar{o},\epsilon} > 0$ is the optimal triggering threshold given by the forthcoming switching-Q-learning algorithm for $\bar{o}(g^{\varsigma}_{r,m}h) = \arg\max_{o\in\mathbb{L}}\{\delta^{\varsigma}_{o(g^{\varsigma}_{r,m}h),\epsilon}\}$ and $g^{\varsigma}_{r,m}h$ belonging to the ϵ-th learning interval $[\mu_{\epsilon}h, \mu_{\epsilon+1}h)$ divided in the switching-Q-learning algorithm with the initial time $\mu_{\epsilon+1}h = \mu_{\epsilon}h + nh$, $\epsilon\in\mathbb{E} = \{0,1,\ldots,\lfloor\frac{t}{nh}\rfloor, \lfloor\frac{t}{nh}\rfloor+1\}$, the total operation duration t for NSSs (1), and the default step length $m\in\mathbb{N}$, $n\in\mathbb{N}^{+}$, $r\in\mathbb{N}^{+}$.

The switching-Q-learning algorithm for selecting the optimal threshold is constituted by two phases: the learning of candidate thresholds for each subsystem and the selection of optimal thresholds for the switched system on operation intervals.

In the first phase, the learning of candidate thresholds for the l-th subsystem or sub-controller is described as a Markov decision process model containing a five-tuple $(\mathbb{A}, \mathbb{S}^{f}_{l}, \gamma^{f}_{l}, \pi^{f}_{l}, \varphi_{l})$ for ϵ-th step and f-th iteration with $f\in\mathbb{F} = \{0,1,\ldots,F\}$ and $l\in\mathbb{L}$. The details are introduced as follows. The action set $\mathbb{A} = \{a_{\tilde{\iota}} | a_{\tilde{\iota}}\in[\underline{\delta},\bar{\delta}], \tilde{\iota} = 1,\ldots,N\}$ contains a given set of candidate thresholds on $[\underline{\delta},\bar{\delta}]$, where $\underline{\delta}$ and $\bar{\delta}$ are the given maximum and minimum thresholds, N represents the number of elements in $\mathbb{A}$. The set of environmental variables $\mathbb{S}^{f}_{l} = \{s^{f}_{l,\epsilon} = (\varsigma_{l,\epsilon}, a^{f}_{l,\epsilon-1}) | \varsigma_{l,\epsilon} = \varsigma_{l,\epsilon}(\mu_{\epsilon}h), a^{f}_{l,\epsilon-1}\in\mathbb{A}\}$ contains the subsystem or sub-controller output $\varsigma_{l,\epsilon}$ at the initial time $\mu_{\epsilon}h = \mu_{\epsilon-1}h + nh$ for ϵ-th step and the initial action $a^{f}_{l,-1} = \underline{\delta}$. The reward function $\gamma^{f}_{l}(\epsilon) = \bar{\gamma}_{l,\epsilon}(a^{f}_{l,\epsilon} - a^{f}_{l,\epsilon-1})$ represents the reward obtained for the environmental variable $s^{f}_{l,\epsilon}$ to execute action $a^{f}_{l,\epsilon}$, where $\bar{\gamma}_{l,\epsilon}$ is a variable coefficient, $\bar{\gamma}_{l,\epsilon}$ is positive if $\varsigma_{l,\epsilon} > \varsigma_{l,\epsilon-1}$, otherwise $\bar{\gamma}_{l,\epsilon}$ is negative. Policy $\pi^{f}_{l}(a^{f}_{l,\epsilon}|s^{f}_{l,\epsilon})$ is the probability of action $a^{f}_{l,\epsilon}$ executed by environment variable $s^{f}_{l,\epsilon}$ at ϵ-th step. The discount parameter $\varphi_{l}\in[0,1]$ defines the extent of the concern for the long-term reward, the larger φ_{l}, the more emphasis is placed on long-term returns. The Q-learning process of candidate thresholds is partitioned into the following two steps:

(i) For the f-th iteration of l-th subsystem or sub-controller, the environment variable $s^{f}_{l,\epsilon}$ at ϵ-th step is transformed into $s^{f}_{l,\epsilon+1}$ at $(\epsilon+1)$-th step by executing the action $a^{f}_{l,\epsilon}$ according to

$$\pi^{f}_{l}(a^{f}_{l,\epsilon}|s^{f}_{l,\epsilon}) = \begin{cases} \pi^{f}_{l}(a_{M}|s^{f}_{l,\epsilon}) = 1 - \beta^{f} + \frac{\beta^{f}}{N}, \\ \pi^{f}_{l}(a_{\mathrm{e}}|s^{f}_{l,\epsilon}) = \frac{\beta^{f}}{N}. \end{cases} \tag{7}$$

Specifically, a random number $c\in[0,1]$ is generated and if $c > \pi^{f}_{l}(a_{M}|s^{f}_{l,\epsilon})$ then $a^{f}_{l,\epsilon} = a_{M}$, otherwise $a^{f}_{l,\epsilon} = a_{e}$, where $a_{M} = \arg\max_{a_{\tilde{\iota}}} Q^{f}_{l}(s^{f}_{l,\epsilon}, a_{\tilde{\iota}})$, $\forall a_{e}\in\mathbb{A}\backslash\{a_{M}\}$. The exploration rate $0 < \beta^{f} = 1/(1+\mathrm{e}^{f+\bar{\beta}_{l}}) < 1$ with the exploration constant $\bar{\beta}_{l}$ for the l-th subsystem. After that, the reward $\gamma^{f}_{l}(\epsilon)$ can be calculated. Then, the action-value function $Q^{f}_{l}(s^{f}_{l,\epsilon}, a^{f}_{l,\epsilon})$, namely Q-value, is updated in the light of the following formula:

$$Q^{f}_{l}(s^{f}_{l,\epsilon}, a^{f}_{l,\epsilon}) = Q^{f-1}_{l}(s^{f-1}_{l,\epsilon}, a^{f-1}_{l,\epsilon}) + \alpha^{f}_{l}[\varphi_{l}\max_{a_{\tilde{\iota}}} Q^{f-1}_{l}(s^{f-1}_{l,\epsilon+1}, a_{\tilde{\iota}}) + \gamma^{f}_{l}(\epsilon) - Q^{f-1}_{l}(s^{f-1}_{l,\epsilon}, a^{f-1}_{l,\epsilon})], \tag{8}$$

where $Q^{f-1}_{l}(s^{f-1}_{l,\epsilon}, a^{f-1}_{l,\epsilon})$ is the estimated value in the Q-table of the $(f-1)$-th iteration and the initial value $Q^{0}_{l}(s^{0}_{l,\epsilon}, a^{0}_{l,\epsilon}) = 0$, $\max_{a_{\tilde{\iota}}} Q^{f-1}_{l}(s^{f-1}_{l,\epsilon+1}, a_{\tilde{\iota}})$ denotes the Q-value corresponding to the action $a_{\tilde{\iota}}\in\mathbb{A}$ with the highest probability for environment variable $s^{f-1}_{l,\epsilon+1}$, the learning rate $\alpha^{f} = 0.1\cdot(2+\arctan(f-\alpha_{l}))$ belongs to $(0,1)$ with the learning constant α_{l} for the l-th subsystem or sub-controller. The above process is repeated until $\epsilon = \lfloor\frac{t}{nh}\rfloor + 1$, then the learning of the f-th iteration is finished.

(ii) For the l-th subsystem or sub-controller, the process of f-th iteration is repeated until $f = F$. After that, the whole Q-table for all pairs of $(s^{F}_{l,\epsilon}, a_{\tilde{\iota}})$ in the l-th subsystem or sub-controller is returned.

Algorithm 1 Selecting proper $\delta^{\varsigma}_{\bar{o}(g^{\varsigma}_{r,m}h),\epsilon}$ in METMs (3) depending on the switching-Q-learning

Input : $\mathbb{A}, n, F, \bar{\gamma}_{l,\epsilon}, \varphi_l, \bar{\beta}_l, \alpha_l, T, \underline{\delta}, \bar{\delta}, h, N$;
Output: $a^F_{l,\epsilon} = \arg\max_{a_{\bar{\iota}}} Q^F_l(s^F_{l,\epsilon}, a_{\bar{\iota}})$;
for $l = 1, 2, \ldots, \bar{l}$ **do**
  Initialize $Q^0_l(s^0_{l,\epsilon}, a_{\bar{\iota}}) = 0, a_{\bar{\iota}} \in \mathbb{A}, \epsilon \in \mathbb{E}$;
  for $f \in 0, 1, \ldots, F$ **do**
    Initialize $a^f_{l,-1} = \underline{\delta}$;
    for $\epsilon = 0, 1, \ldots, \lfloor \frac{t}{nh} \rfloor + 1$ **do**
      Observe $s^f_{l,\epsilon} = (\varsigma^f_{l,\epsilon}, a^f_{l,\epsilon-1})$;
      Choose $a^f_{l,\epsilon}$ by (7);
      Observe α^f_l, $\gamma^f_l(\epsilon)$ and update $Q^f_l(s^f_{l,\epsilon}, a^f_{l,\epsilon})$ by (8);

Input : all $a^F_{l,\epsilon}$;
Output: $\delta^{\varsigma}_{\bar{o}(g^{\varsigma}_{r,m}h),\epsilon}$;
Initialize $r = 1$, $m = 0$;
while $g^{\varsigma}_{r,m}h \leqslant t$ **do**
  Observe $o(g^{\varsigma}_{r,m}h)$;
  if $\sigma(g^{\varsigma}_{r,m}h) = \phi(g^{\varsigma}_{r,m}h)$ and $g^{\varsigma}_{r,m}h \in [\mu_\epsilon h, \mu_{\epsilon+1}h)$ **then**
    $\delta^{\varsigma}_{\bar{o}(g^{\varsigma}_{r,m}h),\epsilon} \leftarrow a^F_{\sigma(g^{\varsigma}_{r,m}h),\epsilon}$;
  else
    $\delta^{\varsigma}_{\bar{o}(g^{\varsigma}_{r,m}h),\epsilon} \leftarrow \max_{o=\sigma,\phi}\{a^F_{o(g^{\varsigma}_{r,m}h),\epsilon}\}$;
  if Eqs. (4), (5) or (6) do not hold **then**
    $m = m + 1$;
  else
    $r = r + 1$ and $m = 0$;

The first phase is completed after learning the candidate thresholds $\delta^{\varsigma}_{l,\epsilon} = a^F_{l,\epsilon} = \arg\max_{a_{\bar{\iota}}} Q^F_l(s^F_{l,\epsilon}, a_{\bar{\iota}})$ for the l-th candidate subsystem or sub-controller.

In the second phase, the optimal threshold $\delta^{\varsigma}_{\bar{o},\epsilon}$ is selected from the candidate thresholds $\delta^{\varsigma}_{l,\epsilon}$ learned via the first phase. On the basis of $r = 1$, $m = 0$, observe $o(g^{\varsigma}_{r,m}h)$ while $g^{\varsigma}_{r,m}h \leqslant t$ is true. Then if $\sigma(g^{\varsigma}_{r,m}h) = \phi(g^{\varsigma}_{r,m}h)$ and $g^{\varsigma}_{r,m}h \in [\mu_\epsilon h, \mu_{\epsilon+1}h)$, then $\delta^{\varsigma}_{\bar{o},\epsilon}$ assigned by the optimal action $a^F_{\sigma,\epsilon}$ is returned; otherwise $\sigma(g^{\varsigma}_{r,m}h) \neq \phi(g^{\varsigma}_{r,m}h)$, then $\delta^{\varsigma}_{\bar{o},\epsilon}$ is assigned by the optimal action $a^F_{o,\epsilon}$, and record $\delta^{\varsigma}_{\bar{o},\epsilon} = \max_{o=\sigma,\phi}\{\delta^{\varsigma}_{o,\epsilon}\}$. After that, if Eqs. (4), (5) or (6) hold, then $r = r + 1$ and $m = 0$; otherwise, $m = m + 1$, condition $g^{\varsigma}_{r,m}h \leqslant t$ is re-checked. Based on the above, we provide the following Algorithm 1 to select the appropriate triggering threshold $\delta^{\varsigma}_{\bar{o}(g^{\varsigma}_{r,m}h),\epsilon}$. The procedure of the switching-Q-learning algorithm is shown in Figure 1.

In summary, METMs (3) are composed of three stages. (1) In the attack-based stage, if Eq. (4) is satisfied, then a trigger $\varsigma(\bar{t}^{\varsigma}_{r+1}h)$ is arranged at the latest sampling instant $\hbar^{\varsigma}_p$ after the LDDoS attack ending time $h^{\varsigma}_p + d^{\varsigma}_p$ measured by the acknowledgment character technique [8] thus alleviating the asynchronous duration. (2) In the error detection stage, if $\Xi^{\varsigma}(g^{\varsigma}_{r,m}h) > 0$ in (5) is satisfied, then $\varsigma(\hat{t}^{\varsigma}_{r+1}h)$ is released. (3) In the modality matching stage, if $o(g^{\varsigma}_{r,m}h) \neq o(g^{\varsigma}_{r,m}h - h)$ in (6), a trigger $\varsigma(\tilde{t}^{\varsigma}_{r+1}h)$ occurs to shrink the asynchronous duration caused by network delay.

Remark 1. Different from Q-learning algorithms with fixed exploration rate and learning rate, the exploration rate β^f and learning rate α^f of the switching-Q-learning algorithm is designed to change with the iteration number f for l-th subsystem. Specifically, in the decision process, each action is taken using the β^f-greedy strategy, which means that in every learning step ϵ, the action strategy π^f_l has a certain probability $\pi^f_l(a_M|s^f_{l,\epsilon})$ to select the optimal action a_M. However, there is also a small probability $\pi^f_l(a_e|s^f_{l,\epsilon})$ to take a completely random action a_e. In (7), it can be seen that as the iteration number f increases, the exploration rate β^f increases, and then the probability of adopting the optimal action a_M increases. The learning rate α^f used in updating Q-value represents the effect of the previous learning outcome $Q^{f-1}_l(s^{f-1}_{l,\epsilon+1}, a_{\bar{\iota}})$. And according to α^f it can be seen that as iteration number f increases, the larger α^f is, the less the effect of retaining the previous $(f-1)$-th learning.

Remark 2. The switching-Q-learning algorithm is proposed to dynamically select the optimal triggering threshold $\delta^{\varsigma}_{\bar{o},\epsilon}$ in METMs (3) for the switched system on synchronous or asynchronous operation intervals after the learning of candidate thresholds for each candidate subsystem or sub-controller. For the non-switched system, some intelligent algorithms such as Q-learning and A3C [25–27] have been successfully

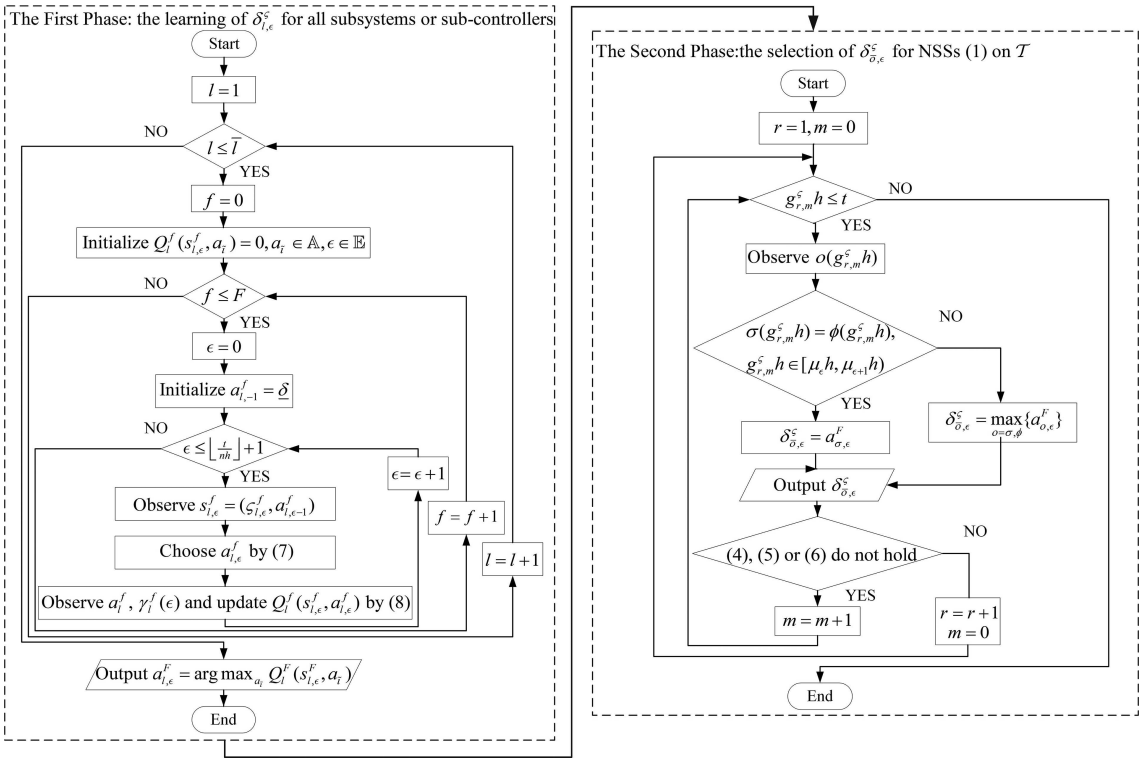

Figure 1 Procedure of the switching-Q-learning algorithm.

applied to choose an optimal triggering threshold. However, when it comes to switched systems, a single Q-table for all subsystems cannot dynamically select the optimal triggering threshold in accordance with the switching behavior. This inspired us to propose the switching-Q-learning algorithm which is divided into two phases. In the first phase, the candidate triggering thresholds are learned for all candidate subsystems or sub-controllers via Q-learning. Then, the second phase selects the optimal triggering thresholds for the activated subsystem or sub-controller among the candidate triggering thresholds via switching-Q-learning. Compared with fixed or pre-given triggering conditions for switched systems, such as [8,20], our improved algorithm calculates the corresponding Q-table on the basis of the switching signal thus intelligently adjusting the triggering thresholds.

2.4 Closed-loop system

The dual networks between the subsystem and sub-controller suffer from transmission delays, so the triggering signal $t^{\varsigma}_r h$ reaches the sub-controller at time $t^{\varsigma}_r h + \tau^{\varsigma}_r$ after the delay τ^{ς}_r. Thus, the interval $\Phi^{\varsigma}_r = [t^{\varsigma}_r h + \tau^{\varsigma}_r, t^{\varsigma}_{r+1} h + \tau^{\varsigma}_{r+1})$ can be divided into $\Phi^{\varsigma}_r = \cup^{\mathfrak{l}^{\varsigma}_r}_{m=0} \Phi^{\varsigma}_{r,m}$, where

$$\Phi^{\varsigma}_{r,m} = \begin{cases} [g^{\varsigma}_{r,m}h + \tau^{\varsigma}_r, g^{\varsigma}_{r,m+1}h + \tau^{\varsigma}_r), \ m = 0, \ldots, \mathfrak{l}^{\varsigma}_r - 1, \\ [g^{\varsigma}_{r,\mathfrak{l}^{\varsigma}_r}h + \tau^{\varsigma}_r, t^{\varsigma}_{r+1}h + \tau^{\varsigma}_{r+1}), \ m = \mathfrak{l}^{\varsigma}_r, \end{cases}$$

with $\mathfrak{l}^{\varsigma}_r = \min\limits_{m \in \mathbb{N}} \{m | g^{\varsigma}_{r,m+1}h + \tau^{\varsigma}_r \geqslant t^{\varsigma}_{r+1}h + \tau^{\varsigma}_{r+1}\}$. Let $\eta^{\varsigma}(t) = t - g^{\varsigma}_{r,m}h$ satisfy the bound $\eta^{\varsigma}_m = \tau^{\varsigma}_m \leqslant \eta^{\varsigma}(t) \leqslant h + \tau^{\varsigma}_M = \eta^{\varsigma}_M$, $\phi(t) = \sigma(t - \eta^y(t))$. Letting $e_{\varsigma}(t) = \varsigma(g^{\varsigma}_{r,m}h) - \varsigma(t^{\varsigma}_r h)$, then the controller input is described as

$$\hat{y}(t) = y(t^y_r h) = y(t - \eta^y(t)) - e_y(t), \quad t \in \Phi^y_{r,m}. \tag{9}$$

After that, the DOFC (2) linked to (3) is recast as

$$\begin{cases} \dot{x}_c(t) = F_\phi x_c(t) + L_\phi x_c(t - \eta^y(t)) + H_\phi \hat{y}(t), \\ \hat{u}(t) = K_\phi x_c(t), \quad t \in \Phi^y_{r,m}. \end{cases} \tag{10}$$

And the input of NSSs (1) with $\hat{u}(t_r^{\hat{u}}h) = \hat{u}(t-\eta^{\hat{u}}(t)) - e_{\hat{u}}(t),\ t \in \Phi_{r,m}^{\hat{u}}$ can be concluded as

$$u(t) = \begin{cases} 0, & t \in \bigcup\limits_{p\in\mathbb{N}^+} \mathbb{H}_p^{\hat{u}}, \\ \hat{u}(t_r^{\hat{u}}h), & t \in \Phi_{r,m}^{\hat{u}} \backslash \bigcup\limits_{p\in\mathbb{N}^+} \mathbb{H}_p^{\hat{u}}. \end{cases} \tag{11}$$

The assumption below is required to obtain the closed-loop system for the SOR of NSSs (1) with (10).

Assumption 3. There exist matrices Λ_σ, Δ_σ, F_ϕ, L_ϕ, K_ϕ such that

$$\begin{cases} A_\sigma\Lambda_\sigma + B_\sigma K_\phi \Delta_\sigma \mathrm{e}^{-G_\sigma \eta_M^{\hat{u}}} + D_\sigma = \Lambda_\sigma G_\sigma, \\ C_\sigma\Lambda_\sigma + E_\sigma = 0, \\ F_\phi\Delta_\sigma + L_\phi\Delta_\sigma \mathrm{e}^{-G_\sigma \eta_M^{y}} = \Delta_\sigma G_\sigma. \end{cases} \tag{12}$$

Substituting (9) and (11) into NSSs (1) under the controller (10), the closed-loop system is written as

$$\begin{cases} \dot{\mathcal{X}}(t) = \tilde{A}_{\sigma,\phi}\mathcal{X}(t) + \tilde{B}_\phi \mathcal{X}(t-\eta^y(t)) + \hat{\Sigma}_{\sigma,\phi} + \tilde{\Sigma}_{\sigma,\phi}, \\ y(t) = \tilde{C}_\sigma \mathcal{X}(t), \end{cases} \tag{13}$$

where $\mathcal{X}(\theta) = \bar{\mathcal{X}}(\theta), \theta \in [-\max\{\eta_M^{\varsigma}\}, 0], \varsigma \in \{y, \hat{u}\}$,

$$\mathcal{X}(t) = \begin{bmatrix} x(t) - \Lambda_\sigma\omega(t) \\ x_c(t) - \Delta_\sigma\omega(t) \end{bmatrix}, \tilde{A}_{\sigma,\phi} = \begin{bmatrix} A_\sigma & 0 \\ 0 & F_\phi \end{bmatrix}, \tilde{B}_\phi = \begin{bmatrix} 0 & 0 \\ 0 & L_\phi \end{bmatrix}, \bar{D}_\phi = \begin{bmatrix} 0 \\ -H_\phi \end{bmatrix},$$

$$\tilde{D}_{\sigma,\phi} = \begin{bmatrix} 0 & 0 \\ C_\sigma H_\phi & 0 \end{bmatrix}, \tilde{E}_{\sigma,\phi} = \begin{bmatrix} 0 & B_\sigma K_\phi \\ 0 & 0 \end{bmatrix}, \bar{E}_\sigma = \begin{bmatrix} -B_\sigma \\ 0 \end{bmatrix}, \tilde{C}_\sigma = [C_\sigma\ 0],$$

$$\hat{\Sigma}_{\sigma,\phi} = \tilde{D}_{\sigma,\phi}\mathcal{X}(t-\eta^y(t)) + \bar{D}_\phi e_y(t), \tilde{\Sigma}_{\sigma,\phi} = \tilde{E}_{\sigma,\phi}\mathcal{X}(t-\eta^{\hat{u}}(t)) + \bar{E}_\sigma e_{\hat{u}}(t).$$

Under the closed-loop system (13), in order to effectively schedule the switching, it is assumed without loss of generality that the k-th, j-th, and i-th subsystems are enabled during adjacent switching intervals $[\ell_{q-2}, \ell_{q-1})$, $[\ell_{q-1}, \ell_q)$, and $[\ell_q, \ell_{q+1})$, and a resilient switching rule is presented as follows:

$$\sigma(t) = \begin{cases} i,\ \{t \in [\ell_q, \ell_q + \mathcal{T}_{\min})\}\ \text{ or }\ \left\{ t \in [\ell_q + \mathcal{T}_{\min}, \ell_q + \mathcal{T}_{\max}) \cap \left\{ t \in \bigcup\limits_{p\in\mathbb{N}^+} \mathbb{H}_p^y\ \text{ or } \mathcal{X}(t) \in \mathcal{D}_i \right\} \right\}, & \text{(14a)} \\ j,\ \left\{ t \in [\ell_q + \mathcal{T}_{\min}, \ell_q + \mathcal{T}_{\max}) \backslash \bigcup\limits_{p\in\mathbb{N}^+} \mathbb{H}_p^y \text{ and } \mathcal{X}(t) \in \mathcal{D}_{ij} \right\}, & \text{(14b)} \\ \arg\min\limits_{j\in\mathbb{L}\backslash i} \{\mathcal{X}^{\mathrm{T}}(t) P_{j\phi(t)} \mathcal{X}(t)\}, \{t = \ell_q + \mathcal{T}_{\max} \text{ and } \mathcal{X}^{\mathrm{T}}(t)(P_{i\phi(t)} + N_{ij})\mathcal{X}(t) \geqslant \mathcal{X}^{\mathrm{T}}(t) P_{j\phi(t)} \mathcal{X}(t)\}, & \text{(14c)} \end{cases}$$

with the initial value $\sigma(\theta) = \arg\min_{i\in\mathbb{L}} \{\mathcal{X}^{\mathrm{T}}(\theta) P_i \mathcal{X}(\theta) | \mathcal{X}(\theta) \in \mathcal{D}_i\}$, where

$$\mathcal{D}_i = \{\mathcal{X}(t) | \mathcal{X}^{\mathrm{T}}(t)(P_{i\phi(t)} - P_{j\phi(t)} + N_{ij})\mathcal{X}(t) < 0, \forall \phi(t) \in \mathbb{L}, \forall j \in \mathbb{L}\backslash i\}, \tag{15}$$

$$\mathcal{D}_{ij} = \{\mathcal{X}(t) | \mathcal{X}^{\mathrm{T}}(t)(P_{i\phi(t)} - P_{j\phi(t)} + N_{ij})\mathcal{X}(t) = 0, \forall \phi(t) \in \mathbb{L}, \forall j \in \mathbb{L}\backslash i\}, \tag{16}$$

and $\mathcal{T}_{\min}$, $\mathcal{T}_{\max}$ are the designed minimum and maximum DTs, respectively, N_{ij} is the indefinite matrix and $\mathcal{X}^{\mathrm{T}}(\ell_0) N_{\sigma(\ell_0)\sigma(\ell_1)} \mathcal{X}(\ell_0) = 0$. Obviously, $\mathcal{D}_{ij}$ is the boundary of $\mathcal{D}_i$ and $\bigcup_{i=1}^{\bar{l}} \mathcal{D}_i = \mathbb{R}^{\mathcal{X}}$, and the proof of the resilient switching rule (14) determining the state-space partition refers to [30].

In accordance with the synchronous or asynchronous model between the subsystem and the controller before ℓ_q, the different launch instant $h_p^y \in [\ell_q, \tilde{\ell}_q)$ or $h_p^y \in [\tilde{\ell}_q, \ell_{q+1})$, and the different duration of LDDoS attacks, the switching of σ and ϕ on any $[\ell_q, \ell_{q+1})$ under the resilient switching rule (14) and METM (3) can be divided into the following cases, as shown in Figure 2.

Case A$_1$. For $\ell_q < h_p^y < h_p^y + d_p^y < \cdots < h_{p+p_q}^y < h_{p+p_q}^y + d_{p+p_q}^y < \tilde{\ell}_q$, the LDDoS attack interval $\mathbb{H}_{\bar{p}}^y \subseteq [\ell_q, \tilde{\ell}_q)$ does not affect the normal controller switching instant $\tilde{\ell}_q$, $\bar{p} \in \{p, \ldots, p+p_q\}$, $p_q \in \mathbb{N}^+$.

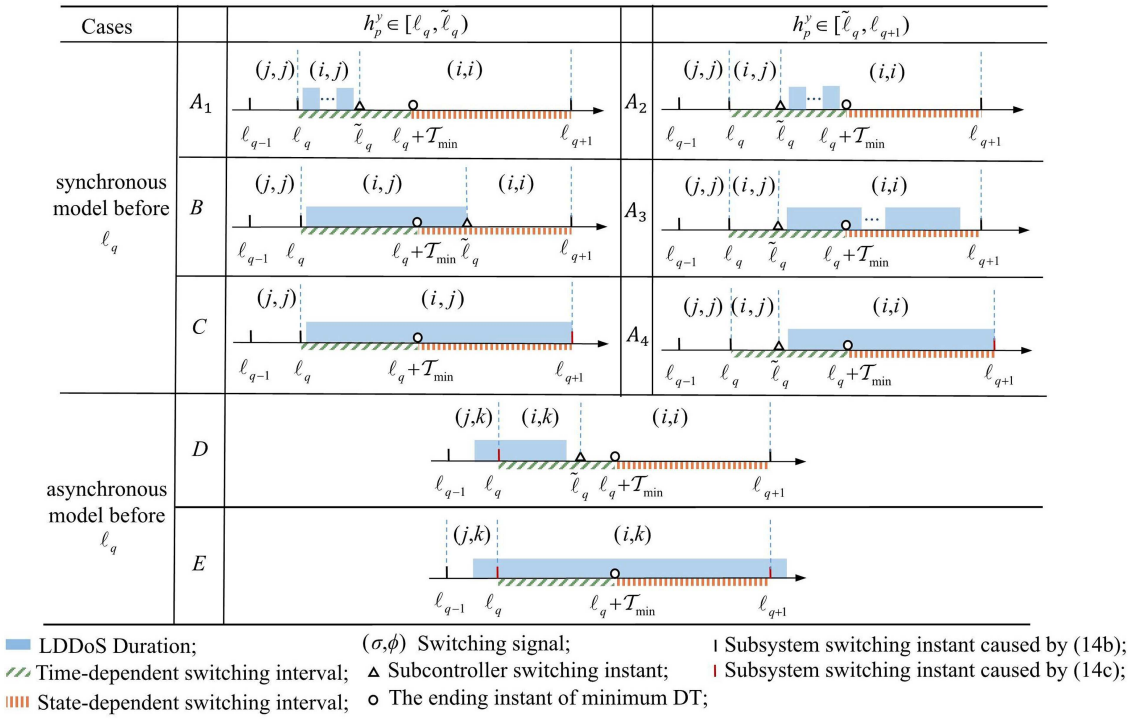

Figure 2 (Color online) Five cases for the closed-loop system (13) with (σ, ϕ).

The attack-based stage (4) and the modality matching stage (6) in METMs reduce the effects of LDDoS attack and network delay on the switching signal after $h_p^y + d_p^y$ and ℓ_q, respectively. Consequently, the controller modality $\phi = j$ is modified to $\phi = i$ at $\tilde{\ell}_q$. Then, the subsystem switches once the resilient switching condition in (14b) is satisfied during $[\ell_q + \mathcal{T}_{\min}, \ell_q + \mathcal{T}_{\max})$.

Case A$_2$. For $\tilde{\ell}_q < h_p^y < h_p^y + d_p^y < \cdots < h_{p+p_q}^y < h_{p+p_q}^y + d_{p+p_q}^y < \ell_q + \mathcal{T}_{\min}$, the attack interval $\mathbb{H}_p^y \subseteq [\tilde{\ell}_q, \ell_q + \mathcal{T}_{\min})$, and the subsystem switching is analogous to Case A$_1$.

Case A$_3$. For $\tilde{\ell}_q < h_p^y < \ell_q + \mathcal{T}_{\min} < h_p^y + d_p^y < \cdots < h_{p+p_q}^y < h_{p+p_q}^y + d_{p+p_q}^y < \ell_q + \mathcal{T}_{\max}$, the activated subsystem $\sigma = i$ is maintained throughout the attack interval $\mathbb{H}_p^y$, then the satisfaction of the resilient switching condition in (14b) is checked.

Case A$_4$. For $\tilde{\ell}_q < h_p^y < \ell_q + \mathcal{T}_{\max} < h_p^y + d_p^y$, the attack interval $\mathbb{H}_p^y$ surpasses the maximum DT of the subsystem $\ell_q + \mathcal{T}_{\max}$, hence the subsystem switching is scheduled at $\ell_q + \mathcal{T}_{\max}$ according to (14c).

By perusing Cases A$_1$–A$_4$ in Figure 2 and the analysis above, it is evident that Cases A$_1$–A$_4$ consider the entire interval or the controller switching instant $\tilde{\ell}_q$ unaffected by the LDDoS attack at different launch and end instants of the attack. Therefore, we can categorize these four sub-cases as Case A, in which their switching signal is summarized as $(\sigma, \phi) = (i, j)$ on $[\ell_q, \tilde{\ell}_q)$ and $(\sigma, \phi) = (i, i)$ on $[\tilde{\ell}_q, \ell_{q+1})$.

Case B. The p-th LDDoS attack interval $\mathbb{H}_p^y$ with $\ell_q < h_p^y < \ell_q + \mathcal{T}_{\min} < h_p^y + d_p^y < \ell_{q+1}$ encompasses the normal controller switching instant $\tilde{\ell}_q$. Owing to the interaction between LDDoS and attack-based stage (4) of METMs, the controller switches at the end of the attack, i.e., $\tilde{\ell}_q = h_p^y + d_p^y$. Then, the switching signal $(\sigma, \phi) = (i, j)$ on $[\ell_q, \tilde{\ell}_q)$ and $(\sigma, \phi) = (i, i)$ on $[\tilde{\ell}_q, \ell_{q+1})$.

Case C. The p-th LDDoS attack interval $\mathbb{H}_p^y$ with $\ell_q < h_p^y < \ell_q + \mathcal{T}_{\max} < h_p^y + d_p^y$ occurs and surpasses $[\ell_q, \ell_{q+1})$. It is clear that $(\sigma, \phi) = (i, j)$ on $[\ell_q, \ell_q + \mathcal{T}_{\max})$.

Case D. The p-th LDDoS attack interval $\mathbb{H}_p^y$ with $\ell_{q-1} < h_p^y < \ell_{q-1} + \mathcal{T}_{\max} < h_p^y + d_p^y$ occurs and does not cover the controller switching instant $\tilde{\ell}_q$, resulting in a consecutive asynchronous of subsystem occurring at $\ell_{q-1} + \mathcal{T}_{\max}$. Apparently, the switching signal $(\sigma, \phi) = (j, k)$ on $[\ell_{q-1}, \ell_{q-1} + \mathcal{T}_{\max})$ and $(\sigma, \phi) = (i, k)$ on $[\ell_{q-1} + \mathcal{T}_{\max}, \tilde{\ell}_q)$.

Case E. The p-th LDDoS attack interval $\mathbb{H}_p^y$ with $\ell_{q-1} < h_p^y < \ell_q + \mathcal{T}_{\max} < h_p^y + d_p^y$ occurs and encompasses the entire interval $[\ell_q, \ell_{q+1})$. It holds that $(\sigma, \phi) = (j, k)$ on $[\ell_{q-1}, \ell_{q-1} + \mathcal{T}_{\max})$ and $(\sigma, \phi) = (i, k)$ on $[\ell_{q-1} + \mathcal{T}_{\max}, \ell_q + \mathcal{T}_{\max})$, in which the consecutive asynchronous of subsystem occurs at $\ell_{q-1} + \mathcal{T}_{\max}$.

Remark 3. The inclusion of the LDDoS attack parameter $\mathbb{H}_p^y$ measured by the ACK technique in the

resilient switching rule (14a) and (14b) exhibits an advantage compared to the existing time-dependent switching rules. For $t\in\bigcup_{p\in\mathbb{N}^+}\mathbb{H}_p^y$, Eq. (14a) retains the activated subsystem and schedules the switching instants at $\ell_q+\mathcal{T}_{\max}$. For $t\notin\bigcup_{p\in\mathbb{N}^+}\mathbb{H}_p^y$, Eq. (14b) schedules the switching to the target subsystem j, which is derived by $\mathcal{D}_{ij}$. For Case B, the inclusion of $\mathbb{H}_p^y$ in the resilient switching rule can effectively eliminate the consecutive asynchronous switching. However, under the time-dependent switching rule in [8], consecutive asynchronous switching inevitably occurs because the attack interval includes the unspecific subsystem switching, which happens at an ambiguous instant after the DT. For Cases A_3, A_4, C, and E, Eq. (14) shrinks the asynchronous duration after $\ell_q+\mathcal{T}_{\max}$ by prolonging the activation intervals of the subsystems during $[\ell_q+\mathcal{T}_{\min},\ell_{q+1})$, while the beginning of the asynchronous interval is advanced to ℓ_{q+1} when Ref. [8] is exploited. Eq. (14) mitigates the impact of asynchronous switching in a more resilient manner than the time-dependent switching rule [8].

Through the analysis of Cases A_1–E, the control objectives are divided into: The closed-loop system (13) with $w(t)=0$ exhibits the mean-square exponential stability; the solution of (13) with $w(t)\neq 0$ meets $\lim_{t\to\infty}y(t)=0$, thus resolving the SOR problem.

3 Main results

Sufficient conditions are deduced by jointly designing DOFC (10), METMs (3), and switching rule (14).

Theorem 1. Under Assumptions 1–3, for given positive constants λ, κ, h, η_m^{ς}, η_M^{ς}, $\rho_i>1$, $0<\mu_i<1$, $i\in\mathbb{L}$, $\varsigma\in\{y,\hat{u}\}$, $\bar{\delta}$, $n_{il}<0$, and parameters $(\vartheta,\bar{\vartheta},\tilde{\vartheta},\hat{o})\in\{(i,i,i,k),(ij,i,j,\lambda),(ik,i,k,\lambda),(jk,j,k,\lambda)\}$ with $i\neq j$, $i\neq k$, $j\neq k$, $i,j,k\in\mathbb{L}$, the SOR of NSSs (1) under LDDoS attacks and network-induced delays is achieved if the forthcoming conditions hold:

(i) There exist matrices $P_\vartheta>0$, $S^{\varpi}>0$, $R^{\varpi}>0$, $\Omega_{\bar{\vartheta}}^{\varsigma,1}>0$, $\Omega_{\bar{\vartheta}}^{\varsigma,2}>0$, and $M^{\tilde{\varpi}}$ with $\varpi\in\{0,1,2,3\}$ and $\tilde{\varpi}\in\{1,3\}$ satisfying

$$\Psi_\vartheta<0, \tag{17}$$

$$\begin{bmatrix} R^{\tilde{\varpi}} & M^{\tilde{\varpi}} \\ * & R^{\tilde{\varpi}} \end{bmatrix}>0. \tag{18}$$

(ii) When the switching of the controller modality ϕ from j to i is unstable, given $\rho_i>1$ such that

$$P_i\leqslant\rho_i P_{ij}, \tag{19}$$

and when the switching is stable, given $0<\mu_i<1$ such that

$$P_i\leqslant\mu_i P_{ij}. \tag{20}$$

(iii) Under the resilient switching rule (14), there exist indefinite matrices N_{ji}, maximum and minimum DTs $\mathcal{T}_{\max}$ and $\mathcal{T}_{\min}$, the number of stable/unstable controller switching n_c^- and n_c^+ as well as $\xi_j\in\{\mu_j,\rho_j,1\}$ meeting the forthcoming conditions:

$$\Gamma_\vartheta\leqslant 0, \tag{21}$$

$$\xi_j N_{kj}+N_{ji}\leqslant 0, \tag{22}$$

$$N_{kj}+N_{ji}\leqslant N_{ki}, \tag{23}$$

$$\eta_M^y+h=\mathcal{T}_{\min}\leqslant\mathcal{T}_{\max}=\frac{-\ln(\bar{\mu}\bar{\rho}\,)}{\max\{\kappa,\lambda\}+(d_{\max}/\tau_d)}, \tag{24}$$

$$\frac{n_c^-}{n_c^+}>-\frac{\ln\bar{\mu}}{\ln\bar{\rho}}, \tag{25}$$

where $\bar{\rho}=\max_{i\in\mathbb{L}}\{\rho_i\}$, $\bar{\mu}=\max_{i\in\mathbb{L}}\{\mu_i\}$, $\bar{\mu}\bar{\rho}<1, \ln(\bar{\mu}\bar{\rho})>(\eta_m^y+h)(\max\{\kappa,\lambda\}+(d_{\max}/\tau_d))$. The $\Psi_\vartheta=\{\psi_\vartheta^{\jmath_1,\jmath_2}\}$ $(\jmath_1,\jmath_2=1,\ldots,9)$ in (17) consists of block matrices:

$$\psi_\vartheta^{11}=\tilde{A}_\vartheta^{\mathrm{T}}P_\vartheta+P_\vartheta\tilde{A}_\vartheta+S^0+S^2-R^0-R^2+3\tilde{A}_\vartheta^{\mathrm{T}}\bar{R}\tilde{A}_\vartheta^{\mathrm{T}}+(2-\hat{o})P_\vartheta+\sum_{l=1}^{\bar{l}}n_{il}(P_{i\tilde{\vartheta}}-P_{l\tilde{\vartheta}}+N_{il}),$$

$$\psi_\vartheta^{12}=P_\vartheta\tilde{B}_{\tilde{\vartheta}}+\tilde{A}_\vartheta^{\mathrm{T}}\bar{R}\tilde{B}_{\tilde{\vartheta}},\psi_\vartheta^{13}=P_\vartheta\tilde{E}_\vartheta+\tilde{A}_\vartheta^{\mathrm{T}}\bar{R}\tilde{E}_\vartheta,\psi_\vartheta^{14}=R^0,\psi_\vartheta^{16}=R^2,\psi_\vartheta^{19}=P_\vartheta\bar{E}_{\bar{\vartheta}}+\tilde{A}_\vartheta^{\mathrm{T}}\bar{R}\bar{E}_{\bar{\vartheta}},$$
$$\psi_\vartheta^{22}=3\tilde{B}_{\tilde{\vartheta}}^{\mathrm{T}}\bar{R}\tilde{B}_{\tilde{\vartheta}}+M^1+M^{1\mathrm{T}}-2R^1+\delta_M^y\tilde{C}_{\tilde{\vartheta}}^{\mathrm{T}}\Omega_{\tilde{\vartheta}}^{y,2}\tilde{C}_{\tilde{\vartheta}}+\tilde{D}_\vartheta^{\mathrm{T}}P_\vartheta\tilde{D}_\vartheta+6\tilde{D}_\vartheta^{\mathrm{T}}\bar{R}\tilde{D}_\vartheta,$$
$$\psi_\vartheta^{23}=\tilde{B}_{\tilde{\vartheta}}^{\mathrm{T}}\bar{R}\tilde{E}_\vartheta,\psi_\vartheta^{24}=R^1-M^{1\mathrm{T}},\psi_\vartheta^{25}=R^1-M^1,\psi_\vartheta^{29}=\tilde{B}_{\tilde{\vartheta}}^{\mathrm{T}}\bar{R}\bar{E}_{\tilde{\vartheta}},$$
$$\psi_\vartheta^{33}=3\tilde{E}_\vartheta^{\mathrm{T}}\bar{R}\tilde{E}_\vartheta+M^3+M^{3\mathrm{T}}-2R^3+\delta_M^{\hat{u}}\mathcal{I}_u^{\mathrm{T}}K_{\tilde{\vartheta}}^{\mathrm{T}}\Omega_{\tilde{\vartheta}}^{\hat{u},2}K_{\tilde{\vartheta}}\mathcal{I}_u,\psi_\vartheta^{36}=R^3-M^{3\mathrm{T}},\psi_\vartheta^{37}=R^3-M^3,$$
$$\psi_\vartheta^{39}=\tilde{E}_\vartheta^{\mathrm{T}}\bar{R}\bar{E}_{\tilde{\vartheta}},\psi_\vartheta^{44}=\mathrm{e}^{\hat{o}\eta_m^y}(S^1-S^0)-R^0-R^1,\psi_\vartheta^{45}=M^1,\psi_\vartheta^{55}=-\mathrm{e}^{\hat{o}\eta_M^y}S^1-R^1,$$
$$\psi_\vartheta^{66}=\mathrm{e}^{\hat{o}\eta_m^{\hat{u}}}(S^3-S^2)-R^2-R^3,\psi_\vartheta^{67}=M^3,\psi_\vartheta^{77}=-\mathrm{e}^{\hat{o}\eta_M^{\hat{u}}}S^3-R^3,\psi_\vartheta^{88}=\bar{D}_{\tilde{\vartheta}}^{\mathrm{T}}P_\vartheta\bar{D}_{\tilde{\vartheta}}+6\bar{D}_{\tilde{\vartheta}}^{\mathrm{T}}\bar{R}\bar{D}_{\tilde{\vartheta}}-\Omega_{\tilde{\vartheta}}^{y,1},$$
$$\psi_\vartheta^{99}=3\bar{E}_{\tilde{\vartheta}}^{\mathrm{T}}\bar{R}\bar{E}_{\tilde{\vartheta}}-\Omega_{\tilde{\vartheta}}^{\hat{u},1},\bar{R}=\sum_{\varpi=0}^{\varpi=3}\tilde{s}^2(\varpi)R^\varpi,\mathcal{I}_u=\left[\begin{smallmatrix}\mathbf{0}\\ *\end{smallmatrix}\ \begin{smallmatrix}\mathbf{0}\\ I\end{smallmatrix}\right],\tilde{s}(\varpi)\in\{\eta_m^y,\eta_M^y-\eta_m^y,\eta_m^{\hat{u}},\eta_M^{\hat{u}}-\eta_m^{\hat{u}}\}.$$

The $\Gamma_\vartheta=\{\Gamma_\vartheta^{\jmath_3,\jmath_4}\}$ ($\jmath_3,\jmath_4=1,\ldots,5$) in (21) consists of block matrices:

$$\Gamma_\vartheta^{11}=\tilde{A}_\vartheta^{\mathrm{T}}N_{ji}+N_{ji}\tilde{A}_\vartheta+(2-\hat{o})N_{ji},\Gamma_\vartheta^{12}=N_{ji}\tilde{B}_{\tilde{\vartheta}},\Gamma_\vartheta^{13}=N_{ji}\tilde{E}_\vartheta,$$
$$\Gamma_\vartheta^{15}=N_{ji}\bar{E}_\vartheta,\Gamma_\vartheta^{22}=\tilde{D}_{\tilde{\vartheta}}^{\mathrm{T}}N_{ji}\tilde{D}_{\tilde{\vartheta}},\Gamma_\vartheta^{33}=-I,\Gamma_\vartheta^{44}=\bar{D}_{\tilde{\vartheta}}^{\mathrm{T}}N_{ji}\bar{D}_{\tilde{\vartheta}},\Gamma_\vartheta^{55}=-I.$$

Proof. To achieve the control objective, we first prove that the closed-loop system (13) with $w(t)=0$ exhibits the mean-square exponential stability and selects the Lyapunov function candidate as

$$V_\vartheta(t)=V_{P_\vartheta}(t)+V_S(t)+V_R(t),\tag{26}$$

where

$$V_{P_\vartheta}(t)=\mathcal{X}^{\mathrm{T}}(t)P_\vartheta\mathcal{X}(t),$$
$$V_S(t)=\sum_{\varpi=0,1,2,3}\int_{t-\underline{s}(\varpi)}^{t-\bar{s}(\varpi)}\mathrm{e}^{\hat{o}(t-s)}S^\varpi(\varpi,s)\mathrm{d}s,$$
$$V_R(t)=\sum_{\varpi=0,1,2,3}\tilde{s}(\varpi)\int_{t-\underline{s}(\varpi)}^{t-\bar{s}(\varpi)}\int_\theta^t\mathrm{e}^{\hat{o}(t-s)}R^\varpi(\varpi,s)\mathrm{d}s\mathrm{d}\theta,$$

with $(\vartheta,\bar{\vartheta},\tilde{\vartheta},\hat{o})\in\{(i,i,i,k),(ij,i,j,\lambda),(ik,i,k,\lambda),(jk,j,k,\lambda)\}$, $S^\varpi(\varpi,\cdot)=\mathcal{X}^{\mathrm{T}}(\cdot)S^\varpi\mathcal{X}(\cdot)$, $R^\varpi(\varpi,\cdot)=\dot{\mathcal{X}}^{\mathrm{T}}(\cdot)R^\varpi\dot{\mathcal{X}}(\cdot)$, $(\bar{s}(\varpi),\underline{s}(\varpi),\tilde{s}(\varpi),\varpi)\in\{(0,\eta_m^y,\eta_m^y,0),(\eta_m^y,\eta_M^y,\eta_M^y-\eta_m^y,1),(0,\eta_m^{\hat{u}},\eta_m^{\hat{u}},2),(\eta_m^{\hat{u}},\eta_M^{\hat{u}},\eta_M^{\hat{u}}-\eta_m^{\hat{u}},3)\}$, and $\hat{o}=\kappa$ if $\sigma=\phi$, else $\hat{o}=\lambda$. Calculating the time derivative of $V_\vartheta(t)$ along the closed-loop system (13) yields

$$\dot{V}_{p_\vartheta}(t)=2\mathcal{X}^{\mathrm{T}}(t)P_\vartheta\dot{\mathcal{X}}(t),$$
$$\dot{V}_S(t)=\hat{o}V_S(t)+\sum_{\varpi=0,2}S^\varpi(\varpi,t)+\sum_{\tilde{\varpi}=1,3}\mathrm{e}^{\hat{o}\bar{s}(\tilde{\varpi})}S^{\tilde{\varpi}}(\tilde{\varpi},t-\bar{s}(\tilde{\varpi}))+\sum_{\varpi=0,1,2,3}\mathrm{e}^{\hat{o}\underline{s}(\varpi)}S^\varpi(\varpi,t-\underline{s}(\varpi)),$$
$$\dot{V}_R(t)=\hat{o}V_R(t)+\sum_{\varpi=0,1,2,3}\left[\tilde{s}^2(\varpi)R^\varpi(\varpi,t)-\tilde{s}(\varpi)\int_{t-\underline{s}(\varpi)}^{t-\bar{s}(\varpi)}\mathrm{e}^{\hat{o}(t-s)}R^\varpi(\varpi,s)\mathrm{d}s\right].$$

Applying [31] to the integral term in $\dot{V}_\vartheta(t)$ and then blending it with $\sum_{l=1}^{\bar{l}}n_{il}\mathcal{X}^{\mathrm{T}}(t)(P_{i\tilde{\vartheta}}-P_{l\tilde{\vartheta}}+N_{il})\mathcal{X}(t)$ from (14) and $n_{ij}<0$ yield

$$\dot{V}_\vartheta(t)-\hat{o}V_\vartheta(t)\leqslant\varepsilon^{\mathrm{T}}(t)\Psi_\vartheta\varepsilon(t),\tag{27}$$

where $\varepsilon^{\mathrm{T}}(t)=[\mathcal{X}^{\mathrm{T}}(t)\ \ \mathcal{X}^{\mathrm{T}}(t-\eta^y(t))\ \ \mathcal{X}^{\mathrm{T}}(t-\eta^{\hat{u}}(t))\ \ \mathcal{X}^{\mathrm{T}}(t-\eta_m^y)\ \ \mathcal{X}^{\mathrm{T}}(t-\eta_M^y)\ \ \mathcal{X}^{\mathrm{T}}(t-\eta_m^{\hat{u}})\ \ \mathcal{X}^{\mathrm{T}}(t-\eta_M^{\hat{u}})\ \ e_{\hat{u}}^{\mathrm{T}}(t)\ \ e_y^{\mathrm{T}}(t)]$.

The following proof discusses the variation of $V(t)$ on the non-switching interval $[\ell_{q-1},\ell_q)\cup[\ell_q,\ell_{q+1})$ according to Cases A–E in Section 2.

Case A. For $t\in[\ell_q,\ell_{q+1})$, this case is divided into asynchronous interval $[\ell_q,\tilde{\ell}_q)$ with $(\sigma,\phi)=(i,j)$, and synchronous interval $t\in[\tilde{\ell}_q,\ell_{q+1})$ with $(\sigma,\phi)=(i,i)$.

For $t\in[\ell_q,\tilde{\ell}_q)$, from (12), we can get $\Psi_{ij}<0$. Then, integrating (27) over $[\ell_q,\tilde{\ell}_q)$ leads to

$$V_{ij}(t)\}\leqslant e^{\lambda(t-\ell_q)}V_{ij}(\ell_q).\tag{28}$$

For $t\in[\tilde{\ell}_q,\ell_q+\mathcal{T}_{\min})$ and $t\in[\ell_q+\mathcal{T}_{\min},\ell_{q+1})$, $\phi(t)=\sigma(t)=i$. Referring to $t\in[\ell_q,\tilde{\ell}_q)$, we can get

$$V_i(t)\leqslant \mathrm{e}^{\kappa(t-\tilde{\ell}_q)}V_i(\tilde{\ell}_q), \tag{29}$$

$$V_i(t)\leqslant \mathrm{e}^{\kappa(t-\ell_q-\mathcal{T}_{\min})}V_i(\ell_q+\mathcal{T}_{\min}). \tag{30}$$

Case B. For $t\in[\ell_q,\ell_{q+1})$, it holds that $(\sigma,\phi)=(i,j)$ on $[\ell_q,\tilde{\ell}_q)$, and $(\sigma,\phi)=(i,i)$ on $[\tilde{\ell}_q,\ell_{q+1})$. Similar to Case A, we can derive (28)–(30).

Case C. For $t\in[\ell_{q-1},\ell_{q+1})$, it holds that $(\sigma,\phi)=(j,k)$ on $[\ell_{q-1},\tilde{\ell}_{q-1})$, $(\sigma,\phi)=(j,j)$ on $[\tilde{\ell}_{q-1},\ell_{q-1}+\mathcal{T}_{\max})$, and $(\sigma,\phi)=(i,j)$ on $[\ell_{q-1}+\mathcal{T}_{\max},\ell_q+\mathcal{T}_{\max})$. Then similar to $[\tilde{\ell}_q,\ell_{q+1})$ of Case A, we can get

$$V_j(t)\leqslant \mathrm{e}^{\kappa(t-\tilde{\ell}_{q-1})}V_j(\tilde{\ell}_{q-1}). \tag{31}$$

Similar to $t\in[\ell_q,\tilde{\ell}_q)$ of Case A, we can obtain

$$V_{jk}(t)\leqslant \mathrm{e}^{\lambda(t-\ell_{q-1})}V_{jk}(\ell_{q-1}), \tag{32}$$

$$V_{ij}(t)\leqslant \mathrm{e}^{\lambda(t-\ell_{q-1}+\mathcal{T}_{\max})}V_{ij}(\ell_{q-1}+\mathcal{T}_{\max}). \tag{33}$$

Case D. For $t\in[\ell_{q-1},\ell_{q+1})$, it holds that $(\sigma,\phi)=(j,k)$ on $[\ell_{q-1},\ell_{q-1}+\mathcal{T}_{\max})$, $(\sigma,\phi)=(i,k)$ on $[\ell_{q-1}+\mathcal{T}_{\max},\tilde{\ell}_q)$, and $(\sigma,\phi)=(i,i)$ on $[\tilde{\ell}_q,\ell_{q+1})$. Similar to Case A, we can derive

$$V_{ij}(t)\leqslant \mathrm{e}^{\lambda(t-\ell_{q-1}+\mathcal{T}_{\max})}V_{ij}(\ell_{q-1}+\mathcal{T}_{\max}), \tag{34}$$

$$V_i(t)\leqslant \mathrm{e}^{\kappa(t-\tilde{\ell}_q)}V_i(\tilde{\ell}_q). \tag{35}$$

Case E. For $t\in[\ell_{q-1},\ell_{q+1})$, it holds that $(\sigma,\phi)=(j,k)$ on $[\ell_{q-1},\ell_{q-1}+\mathcal{T}_{\max})$ and $(\sigma,\phi)=(i,k)$ on $[\ell_{q-1}+\mathcal{T}_{\max},\ell_q+\mathcal{T}_{\max})$. Then similar to $t\in[\ell_q,\tilde{\ell}_q)$ of Case A, we can derive

$$V_{jk}(t)\leqslant \mathrm{e}^{\lambda(t-\ell_{q-1})}V_{jk}(\ell_{q-1}), \tag{36}$$

$$V_{ik}(t)\leqslant \mathrm{e}^{\lambda(t-\ell_{q-1}-\mathcal{T}_{\max})}V_{ik}(\ell_{q-1}+\mathcal{T}_{\max}). \tag{37}$$

For any non-switching interval $[\ell_q,\ell_{q+1})$, the variation of $\mathcal{X}^{\mathrm{T}}(t)N_{ji}\mathcal{X}(t)$ along the closed-loop system (13) is discussed. For the subsystem switching instant $\ell_q\in\mathcal{L}_s$ under the switching rule (14b), it satisfies

$$V_{ij}(\ell_q^+)=V_j(\ell_q^-)+\mathcal{X}^{\mathrm{T}}(\ell_q)N_{ji}\mathcal{X}(\ell_q). \tag{38}$$

For $\ell_q\in\mathcal{L}_s$ under the switching rule (14c), we can obtain

$$V_{ij}(\ell_q^+)\leqslant V_j(\ell_q^-)+\mathcal{X}^{\mathrm{T}}(\ell_q)N_{ji}\mathcal{X}(\ell_q). \tag{39}$$

Calculating the differential of $\mathcal{X}^{\mathrm{T}}(\ell_q)N_{ji}\mathcal{X}(\ell_q)$ along the trajectory of (13) results in Γ_ϑ in $[\ell_q,\ell_{q+1})$.

Next, the progression of $V(t)$ is discussed at $\tilde{\ell}_q$. For $\tilde{\ell}_q\in\mathcal{L}_c^-$ under (20), one can obtain

$$V_i(\tilde{\ell}_q^+)\leqslant \mu_i V_{ij}(\tilde{\ell}_q^-)\leqslant \bar{\mu}V_{ij}(\tilde{\ell}_q^-). \tag{40}$$

For $\tilde{\ell}_q\in\mathcal{L}_c^+$ under (19), one can derive

$$V_i(\tilde{\ell}_q^+)\leqslant \rho_i V_{ij}(\tilde{\ell}_q^-)\leqslant \bar{\rho}V_{ij}(\tilde{\ell}_q^-). \tag{41}$$

Subsequently, we discuss the relationship between $V(t)$ and $V(\ell_{q-1})$ in Cases A–E through the above analysis of the variation of $V(t)$ in the interval $[\ell_{q-1},\ell_q)\cup[\ell_q,\ell_{q+1})$, with switching instants ℓ_q and $\tilde{\ell}_q$.

The switching behaviors in Cases A_1–A_4 have been summarized as Case A by recalling the statement in Subsection 2.4. For this case, in virtue of (29), (30), (40) and (41), it holds that

$$V(t)=V_i(t)\leqslant \xi_i\mathrm{e}^{\kappa(t-\tilde{\ell}_q)}V_i(\tilde{\ell}_q^-). \tag{42}$$

With the help of (28), it can be deduced that $V_i(\tilde{\ell}_q^-)\leqslant \mathrm{e}^{\lambda(\tilde{\ell}_q-\ell_q)}V_{ij}(\ell_q^+)$. After that, it follows from (38) that $V_{ij}(\ell_q^+)=V_j(\ell_q^-)+\mathcal{X}^{\mathrm{T}}(\ell_q^-)N_{ji}\mathcal{X}(\ell_q^-)$. On the one hand, the similar procedure to deal with the change

of $V_j(\ell_q^-)$ on $[\ell_{q-1},\ell_q)$ leads to $V_j(\ell_q^-)\leqslant \xi_j \mathrm{e}^{\kappa(\ell_q-\tilde{\ell}_{q-1})}\mathrm{e}^{\lambda(\tilde{\ell}_{q-1}-\ell_{q-1})}V_k(\ell_{q-1}^-)+\mathcal{X}^{\mathrm{T}}(\ell_{q-1}^-)N_{kj}\mathcal{X}(\ell_{q-1}^-)$. On the other hand, $\Gamma_i\leqslant 0$ and $\Gamma_{ij}\leqslant 0$ can be deduced from (21), which leads to $\mathcal{X}^{\mathrm{T}}(\ell_q^-)N_{ji}\mathcal{X}(\ell_q^-)\leqslant \mathrm{e}^{\kappa(\ell_q-\tilde{\ell}_{q-1})}\mathrm{e}^{\lambda(\tilde{\ell}_{q-1}-\ell_{q-1})}\mathcal{X}^{\mathrm{T}}(\ell_{q-1}^-)N_{ji}\mathcal{X}(\ell_{q-1}^-)$ on $[\ell_{q-1},\ell_q)$. Then, combining it with $\mathcal{X}^{\mathrm{T}}(\ell_{q-1}^-)N_{kj}\mathcal{X}(\ell_{q-1}^-)$ yields $\mathcal{X}^{\mathrm{T}}(\ell_{q-1}^-)(\xi_j N_{kj}+N_{ji})\mathcal{X}(\ell_{q-1}^-)\leqslant 0$ according to (22). Therefore, Eq. (42) can be arranged as

$$\begin{aligned}V(t)=V_i(t)&\leqslant \xi_j\xi_i\mathrm{e}^{\kappa(t-\tilde{\ell}_q+\ell_q-\tilde{\ell}_{q-1})}\mathrm{e}^{\lambda(\tilde{\ell}_q-\ell_q+\tilde{\ell}_{q-1}-\ell_{q-1})}V_k(\ell_{q-1}^-)\\&\leqslant \bar{\mu}^{q_3(\ell_{q-1},t)}\bar{\rho}^{q_4(\ell_{q-1},t)}\mathrm{e}^{\kappa\mathcal{T}_s(\ell_{q-1},t)+\lambda\mathcal{T}_{as}(\ell_{q-1},t)}V_k(\ell_{q-1}^-).\end{aligned}\tag{43}$$

For Case B, due to the LDDoS attack, it is apparent that the controller switching instant $\tilde{\ell}_q=h_p^y+d_p^y$ holds. The rest of the deduction is comparable to Case A, and with the help of $\Gamma_i\leqslant 0$ and $\Gamma_{ij}\leqslant 0$ we can deduce

$$V(t)=V_i(t)\leqslant \bar{\mu}^{q_3(\ell_{q-1},t)}\bar{\rho}^{q_4(\ell_{q-1},t)}\mathrm{e}^{\kappa\mathcal{T}_s(\ell_{q-1},t)+\lambda\mathcal{T}_{as}(\ell_{q-1},t)}V_k(\ell_{q-1}^-).\tag{44}$$

For Case C, the switching signal (σ,ϕ) is (i,j) on $[\ell_{q-1}+\mathcal{T}_{\max},\ell_q+\mathcal{T}_{\max})$, and we deduce $V(t)=V_{ij}(t)\leqslant \mathrm{e}^{\lambda(t-\ell_{q-1}+\mathcal{T}_{\max})}V_{ij}(\ell_q^+)$ from (33). Then the following steps are similar to Case A, which provides from $\Gamma_{ij}\leqslant 0$ and (38)–(41) that

$$\begin{aligned}V(t)=V_i(t)&\leqslant \xi_j\mathrm{e}^{\lambda(t-\ell_{q-1}+\mathcal{T}_{\max}+\tilde{\ell}_{q-1}-\ell_{q-1})}\mathrm{e}^{\kappa(\ell_q-\tilde{\ell}_{q-1})}V_k(\ell_{q-1}^-)\\&\leqslant \bar{\mu}^{q_3(\ell_{q-1},t)}\bar{\rho}^{q_4(\ell_{q-1},t)}\mathrm{e}^{\kappa\mathcal{T}_s(\ell_{q-1},t)+\lambda\mathcal{T}_{as}(\ell_{q-1},t)}V_k(\ell_{q-1}^-).\end{aligned}\tag{45}$$

For Case D, Eq. (42) can be obtained from (35), (40), and (41). However, different from Cases A and B, on the interval $[\ell_{q-1}+\mathcal{T}_{\max},\tilde{\ell}_q)$, the switching signal (σ,ϕ) is (i,k). So in aid of (34), we can obtain $V_i(\tilde{\ell}_q^-)\leqslant \mathrm{e}^{\lambda(\tilde{\ell}_q-\ell_{q-1}+\mathcal{T}_{\max})}V_{ik}(\ell_q^+)$. Then via $\Gamma_{ik}\leqslant 0$, $\Gamma_i\leqslant 0$, and (39), we get $V_{ik}(\ell_q^+)\leqslant V_{jk}(\ell_q^-)+\mathcal{X}^{\mathrm{T}}(\ell_q^-)N_{ji}\mathcal{X}(\ell_q^-)$, where $V_{jk}(\ell_q^-)\leqslant \mathrm{e}^{\lambda(\ell_{q-1}+\mathcal{T}_{\max}-\ell_{q-1})}\,V_k\,(\ell_{q-1}^-)+\mathcal{X}^{\mathrm{T}}(\ell_{q-1}^-)N_{kj}\mathcal{X}(\ell_{q-1}^-)$ and $\mathcal{X}^{\mathrm{T}}(\ell_{q-1}^-)(N_{kj}+N_{ji})\mathcal{X}(\ell_{q-1}^-)\leqslant 0$. Therefore, Eq. (42) becomes

$$\begin{aligned}V(t)=V_i(t)&\leqslant \xi_i\mathrm{e}^{\kappa(t-\tilde{\ell}_q)}\mathrm{e}^{\lambda(\tilde{\ell}_q-\ell_{q-1})}V_k(\ell_{q-1}^-)\\&\leqslant \bar{\mu}^{q_3(\ell_{q-1},t)}\bar{\rho}^{q_4(\ell_{q-1},t)}\mathrm{e}^{\kappa\mathcal{T}_s(\ell_{q-1},t)+\lambda\mathcal{T}_{as}(\ell_{q-1},t)}V_k(\ell_{q-1}^-).\end{aligned}\tag{46}$$

For Case E, the switching signal (σ,ϕ) is (i,k) on $[\ell_{q-1}+\mathcal{T}_{\max},\ell_q+\mathcal{T}_{\max})$, so $V(t)=V_{ik}(t)\leqslant \mathrm{e}^{\lambda(t-\ell_{q-1}+\mathcal{T}_{\max})}V_{ik}(\ell_q^+)$ can be derived from (36) and (37). The following processing steps are similar to Case D, under (39) and $\Gamma_{ik}\leqslant 0$, the formula above becomes

$$\begin{aligned}V(t)=V_{ik}(t)&\leqslant \mathrm{e}^{\lambda(t-\ell_{q-1})}V_k(\ell_{q-1}^-)\\&\leqslant \bar{\mu}^{q_3(\ell_{q-1},t)}\bar{\rho}^{q_4(\ell_{q-1},t)}\mathrm{e}^{\lambda\mathcal{T}_{as}(\ell_{q-1},t)}V_k(\ell_{q-1}^-).\end{aligned}\tag{47}$$

Summarizing the variation of $V(t)$ in (43)–(47) in Cases A–E on $[\ell_{q-1},\ell_{q+1})$ can deduce

$$V(t)\leqslant \bar{\mu}^{q_3(\ell_{q-1},t)}\bar{\rho}^{q_4(\ell_{q-1},t)}\mathrm{e}^{\kappa\mathcal{T}_s(\ell_{q-1},t)+\lambda\mathcal{T}_{as}(\ell_{q-1},t)}V_k(\ell_{q-1}^-).\tag{48}$$

Subsequently, combining the analysis of the variation of $V(t)$ on the interval $[\ell_{q-1},\ell_{q+1})$ as discussed in Cases A–E, the relationship between $V(t)$ and $V(\ell_0)$ over $[0,t)$ can be derived as follows:

$$\begin{aligned}V(t)&\leqslant \bar{\mu}^{q_3(\ell_{q-1},t)}\bar{\rho}^{q_4(\ell_{q-1},t)}\mathrm{e}^{\kappa\mathcal{T}_s(\ell_{q-1},t)+\lambda\mathcal{T}_{as}(\ell_{q-1},t)}V_k(\ell_{q-1}^-)\\&\leqslant\cdots\leqslant \bar{\mu}^{n_c^-}\bar{\rho}^{n_c^+}\mathrm{e}^{[\kappa\mathcal{T}_s(0,t)+\lambda\mathcal{T}_{as}(0,t)]}V_{\sigma(\ell_0)}(\ell_0),\end{aligned}$$

if q is odd, and if q is even it can be concluded via $\mathcal{X}^{\mathrm{T}}(\ell_0)N_{\sigma(\ell_0)\sigma(\ell_1)}\mathcal{X}(\ell_0)=0$ that

$$\begin{aligned}V(t)&\leqslant \bar{\mu}^{q_3(\ell_{q-1},t)}\bar{\rho}^{q_4(\ell_{q-1},t)}\mathrm{e}^{\kappa\mathcal{T}_s(\ell_{q-1},t)+\lambda\mathcal{T}_{as}(\ell_{q-1},t)}V_k(\ell_{q-1}^-)\\&\leqslant\cdots\bar{\mu}^{n_c^-}\bar{\rho}^{n_c^+}\mathrm{e}^{[\kappa\mathcal{T}_s(0,t)+\lambda\mathcal{T}_{as}(0,t)]}V_{\sigma(\ell_0)}(\ell_0)+\chi^{\mathcal{T}}(\ell_0)N_{\sigma(\ell_0)\sigma(\ell_1)}\chi(\ell_0)\\&\leqslant \bar{\mu}^{n_c^-}\bar{\rho}^{n_c^+}\mathrm{e}^{[\kappa\mathcal{T}_s(0,t)+\lambda\mathcal{T}_{as}(0,t)]}V_{\sigma(\ell_0)}(\ell_0).\end{aligned}$$

Then, the relationship between $V(t)$ and $V(\ell_0)$ can be summarized as

$$V(t)\leqslant \bar{\mu}^{n_c^-}\bar{\rho}^{n_c^+}\mathrm{e}^{[\kappa\mathcal{T}_s(0,t)+\lambda\mathcal{T}_{as}(0,t)]}V_{\sigma(\ell_0)}(\ell_0),\tag{49}$$

where $\mathcal{T}_s(0,t)$ and $\mathcal{T}_{as}(0,t)$ are total synchronous and asynchronous switching durations over $[0,t)$. Significantly, since $0 < d_{\max}N_d(0,t)$, it can be deduced that $\kappa\mathcal{T}_s(0,t)+\lambda\mathcal{T}_{as}(0,t) \leqslant \max\{\kappa,\lambda\}t + d_{\max}N_d(0,t)$, and then taking advantage of $t \leqslant N_\sigma\mathcal{T}_{\max}$ and Assumption 1, we deduce $\max\{\kappa,\lambda\}t + d_{\max}N_d(0,t) \leqslant \max\{\kappa,\lambda\}N_\sigma\mathcal{T}_{\max} + d_{\max}(\omega_d + \mathcal{T}_{\max}(N_\sigma/\tau_d))$. Furthermore, on the basis of $n_s^- + n_s^+ = N_\sigma$ and (25), one can infer $n_c^-\ln\bar{\mu} + n_c^+\ln\bar{\rho} \leqslant N_\sigma(\ln\bar{\mu}+\ln\bar{\rho}) - (n_s^- + n_s^+ - n_c^-)\ln\bar{\mu} - n_c^-\ln\bar{\rho} \leqslant N_\sigma(\ln\bar{\mu}+\ln\bar{\rho})$. Based on the above analysis, it holds that $n_c^-\ln\bar{\mu} + n_c^+\ln\bar{\rho} + \kappa\mathcal{T}_s(0,t) + \lambda\mathcal{T}_{as}(0,t) \leqslant N_\sigma(\ln\bar{\rho} - \ln\bar{\mu}) + \max\{\kappa,\lambda\}N_\sigma\mathcal{T}_{\max} + d_{\max}\mathcal{T}_{\max}(N_\sigma/\tau_d\,) + d_{\max}\omega_d$. Thus, Eq. (49) can be rewritten as

$$V(t) \leqslant d\mathrm{e}^{Zt}V_{\sigma(\ell_0)}(\ell_0), \tag{50}$$

where $d = \mathrm{e}^{d_{\max}\omega_d}$, $Z = [\ln\bar{\mu} + \ln\bar{\rho} + \max\{\kappa,\lambda\}\mathcal{T}_{\max} + (d_{\max}/\tau_d\,)\mathcal{T}_{\max}]N_\sigma/(\mathcal{T}_{\max}(n_s^- + n_s^+)) < 0$, and Eq. (24) shows $Z < 0$. It can be inferred from (26) and (50) that

$$||\mathcal{X}(t)||^2 \leqslant \frac{\tilde{b}}{\tilde{a}}d\mathrm{e}^{Zt}||\mathcal{X}(0)||^2, \tag{51}$$

where $\tilde{a} = \min_{\vartheta\in\mathbb{L}\times\mathbb{L}}\{\lambda_m(P_\vartheta)\}$, $\tilde{b} = \max_{\vartheta\in\mathbb{L}\times\mathbb{L}}\{\lambda_M(P_\vartheta + \sum_{\varpi=0}^{\varpi=3}[\tilde{s}(\varpi)S^\varpi + \underline{s}^2(\varpi)R^\varpi])\}$, indicating that the closed-loop system (13) with $w(t)=0$ exhibits the mean-square exponential stability.

In accordance with the center manifold theory [32], there are positive scalars $\hat{Z}$ and $\hat{d}$ that result in $||x(t) - \Lambda_\sigma w(t)|| + ||x_c(t) - \Delta_\sigma w(t)|| \leqslant \hat{d}\mathrm{e}^{-\hat{Z}t}||x(0) - \Lambda_\sigma w(0)|| + ||x_c(0) - \Delta_\sigma w(0)||$, which proves the solution of (13) with $w(t)\neq 0$ meets $\lim_{t\to\infty} y(t) = 0$.

Remark 4. The switching instants of the subsystem and the controller allow the increase of adjacent Lyapunov functions, due to the introduction of N_{ji} in (14) and ρ_i in (19). For subsystem switching, $V(\ell_q)$ is allowed to be jumpable upward or downward; that is, there exists the stable switching ℓ_q^- and unstable switching ℓ_q^+ according to (22) and (23) in which the N_{ji} is not required to be positive definite or negative definite and $\mathcal{X}^{\mathrm{T}}(P_j - P_{ij} + N_{ji})\mathcal{X} = 0$. For controller switching, $V(\tilde{\ell}_q)$ can be jumpable upward, that is, unstable switching $\tilde{\ell}_q^+$, which is promised by $\rho_i > 1$ in (19). In addition, the increments and decrements at switching instants remain uncorrelated with each other, relaxing the constraints in [8].

In what follows, the linearization of the nonlinear terms Ψ_ϑ and Γ_ϑ in Theorem 1 yields the forthcoming linear matrix inequality conditions.

Theorem 2. Under Assumptions 1–3, given positive constants λ, κ, h, η_m^ς, η_M^ς, $\rho_i > 1$, $0 < \mu_i < 1$, $i \in \mathbb{L}$, $\varsigma \in \{y, \hat{u}\}$, $\bar{\delta}$, $n_{il} < 0$ and parameters $(\vartheta,\bar{\vartheta},\tilde{\vartheta},\hat{o}) \in \{(i,i,i,k),(ij,i,j,\lambda),(ik,i,k,\lambda),(jk,j,k,\lambda)\}$ with $i \neq j \neq k$, $i,j,k \in \mathbb{L}$. If conditions (18)–(20) and (22)–(25) in Theorem 1 hold and there exist matrices $P_\vartheta > 0$, $S^\varpi > 0$, $R^\varpi > 0$, $\Omega_\vartheta^{\varsigma,1} > 0$, $\Omega_\vartheta^{\varsigma,2} > 0$, $M^{\tilde{\varpi}}$, $\varpi \in \{0,1,2,3\}$, and $\tilde{\varpi} \in \{1,3\}$ satisfying

$$\tilde{\Psi}_\vartheta < 0, \tag{52}$$

$$\tilde{\Gamma}_\vartheta < 0, \tag{53}$$

then, the SOR for NSSs (1) under LDDoS attacks and network-induced delays is solvable, where the $\tilde{\Psi}_\vartheta = \{\tilde{\psi}_\vartheta^{\jmath_5,\jmath_6}\}$ ($\jmath_5, \jmath_6 = 1,\ldots,11$) in (52) is composed of block matrices:

$$\tilde{\psi}_\vartheta^{22} = 3\tilde{B}_{\tilde{\vartheta}}^{\mathrm{T}}\bar{R}\tilde{B}_{\tilde{\vartheta}} + M^1 + M^{1\mathrm{T}} - 2R^1 + \delta_M^y\tilde{C}_{\tilde{\vartheta}}^{\mathrm{T}}\Omega_{\tilde{\vartheta}}^{y,2}\tilde{C}_{\tilde{\vartheta}}, \tilde{\psi}_\vartheta^{2,10} = \tilde{D}_\vartheta^{\mathrm{T}}, \tilde{\psi}_\vartheta^{33} = 3\tilde{E}_\vartheta^{\mathrm{T}}\bar{R}\tilde{E}_\vartheta + M^3 + M^{3\mathrm{T}} - 2R^3,$$
$$\tilde{\psi}_\vartheta^{88} = -\Omega_{\tilde{\vartheta}}^{y,1}, \tilde{\psi}_\vartheta^{8,11} = \bar{D}_{\tilde{\vartheta}}^{\mathrm{T}}, \tilde{\psi}_\vartheta^{10,10} = \tilde{\psi}_\vartheta^{11,11} = \bar{\omega}^2(P_{\bar{\vartheta}} + 6\bar{R}) - 2\bar{\omega}I;$$

the $\tilde{\Gamma}_\vartheta = \{\tilde{\Gamma}_\vartheta^{\jmath_7,\jmath_8}\}$ ($\jmath_7, \jmath_8 = 1,\ldots,7$) in (53) consists of block matrices $\tilde{\Gamma}_\vartheta^{2,6} = \tilde{D}_{\tilde{\vartheta}}^{\mathrm{T}}$, $\tilde{\Gamma}_\vartheta^{4,7} = \bar{D}_{\tilde{\vartheta}}^{\mathrm{T}}$, $\tilde{\Gamma}_\vartheta^{6,6} = \tilde{\Gamma}_\vartheta^{7,7} = \bar{\omega}^2N_{ji} - \bar{\omega}I_\vartheta$; block matrices $\tilde{\psi}_\vartheta^{\jmath_5,\jmath_6} = \psi_\vartheta^{\jmath_1,\jmath_2}$ for $\jmath_5, \jmath_6 = 1,\ldots,9$ and $\tilde{\Gamma}_\vartheta^{\jmath_7,\jmath_8} = \Gamma_\vartheta^{\jmath_3,\jmath_4}$ for $\jmath_7, \jmath_8 = 1,\ldots,5$; other block matrices in $\tilde{\Psi}_\vartheta$ and $\tilde{\Gamma}_\vartheta$ are $\mathbf{0}$ with proper dimensions.

Proof. In the beginning, Lemma 2 in [33] is applied to handle the nonlinear term of (24) in Case A as follows: $-(P_{ij} + 6\bar{R})^{-1} < \bar{\omega}^2(P_{ij} + 6\bar{R}) - 2\bar{\omega}I$ and $-(P_i + 6\bar{R})^{-1} < \bar{\omega}^2(P_i + 6\bar{R}) - 2\bar{\omega}I$. Then, with the help of the Schur complement lemma, one can readily get $\tilde{\Psi}_{ij} < 0$, $\tilde{\Gamma}_j < 0$, and $\tilde{\Gamma}_{jk} < 0$ from $\Psi_{ij} < 0$, $\Gamma_j < 0$, and $\Gamma_{jk} < 0$. For Cases B–E, repeating the steps in Case A, we can conclude that $\tilde{\Psi}_\vartheta < 0$ and $\tilde{\Gamma}_\vartheta < 0$. The remaining steps are similar to Theorem 1.

4 Simulation example

The linearized longitudinal short-period motion of the F-18 aircraft can be modeled as NSSs (1), where $x^{\mathrm{T}} = [x_1\ x_2] = [\alpha\ q]$, $u^{\mathrm{T}} = [u_1\ u_2] = [\delta_E\ \delta_{\mathrm{PTV}}]$ and α, q, δ_E, δ_{PTV} are the angle of attack, pitch rate, symmetric elevator position and pitch thrust vectoring nozzle position. A_σ, B_σ are system matrices containing the longitudinal stability derivatives and the longitudinal control derivatives. $\sigma \in \mathbb{L} = \{1, 2, 3\}$ denotes the flight attitude of the aircraft at Mach 0.6 and altitude 30 kft, Mach 0.5 and altitude 40 kft, and Mach 0.7 and altitude 14 kft from [34], respectively,

$$A_1 = \begin{bmatrix} -0.509 & 0.994 \\ -1.131 & -0.280 \end{bmatrix}, A_2 = \begin{bmatrix} -0.242 & 0.996 \\ -2.342 & -0.173 \end{bmatrix}, A_3 = \begin{bmatrix} -1.175 & 0.987 \\ -8.458 & -0.878 \end{bmatrix},$$

$$B_1 = \begin{bmatrix} -0.093 & -0.018 \\ -6.573 & -1.525 \end{bmatrix}, B_2 = \begin{bmatrix} -0.042 & -0.012 \\ -2.595 & -0.816 \end{bmatrix}, B_3 = \begin{bmatrix} -0.194 & -0.036 \\ -19.290 & -3.803 \end{bmatrix}.$$

Other system matrices for SOR are preset as

$$C_1 = \begin{bmatrix} 0.1 & 0 \\ 0 & 0.2 \end{bmatrix}, C_2 = \begin{bmatrix} 0.2 & 0 \\ -0.1 & 0.2 \end{bmatrix}, C_3 = \begin{bmatrix} 0.2 & 0 \\ 0 & 0.2 \end{bmatrix}, D_1 = \begin{bmatrix} 0.12 & 2.39 \\ 0.84 & 0.78 \end{bmatrix}, D_2 = \begin{bmatrix} 0.53 & 1.76 \\ 6.78 & 1.61 \end{bmatrix}, D_3 = \begin{bmatrix} 0.35 & 0.67 \\ 0.19 & 0.87 \end{bmatrix},$$

$$E_1 = \begin{bmatrix} 0.1 & 0.08 \\ 0.1 & 0.05 \end{bmatrix}, E_2 = \begin{bmatrix} 0.2 & 0.06 \\ 0.1 & 0.02 \end{bmatrix}, E_3 = \begin{bmatrix} 0.08 & 0.2 \\ 0.09 & 0.1 \end{bmatrix}, G_1 = \begin{bmatrix} 0.12 & -4 \\ 0.15 & 0.1 \end{bmatrix}, G_2 = \begin{bmatrix} 0.11 & -2.8 \\ 0.23 & 0.22 \end{bmatrix}, G_3 = \begin{bmatrix} -0.1 & -3.1 \\ 0.12 & 0.1 \end{bmatrix}.$$

Select parameters $\lambda = 0.42$, $\kappa = 0.5$, $h = 0.01$, $\eta_m^{\varsigma} = 0.003$, $\eta_M^{\varsigma} = 0.015$, $\mu_i = 0.24$, $\rho_i = 1.1$, $\bar{\delta} = 0.1$, $\omega_d = 4$, $\tau_d = 1.15$, $d_{\max} = 2.5$, $n_{ij} = -1$, $\bar{\omega} = 0.9$, $i, j \in \{1, 2, 3\}$, which results in $\mathcal{T}_{\min} = 0.1$s, $\mathcal{T}_{\max} = 0.498$ s. The parameters of the switching-Q-learning algorithm for training the triggering thresholds of METMs (3) are chosen as follows: $\varphi_l = 0.42$, $n = 1$, $F = 50$, and $\mathbb{A} = [0.02, 0.04, 0.06, 0.08, 0.1]$. $\bar{\beta}_l$ in (7) is chosen as $\bar{\beta}_1 = 3$, $\bar{\beta}_2 = 2$, $\bar{\beta}_3 = 4$ and α_l in (8) is selected as $\alpha_1 = 5$, $\alpha_2 = 4$, $\alpha_3 = 6$. $\bar{\gamma}_{l,\epsilon} = -10$ when $\varsigma_{l,\epsilon} - \varsigma_{l,\epsilon-1} > 0.01$, otherwise $\bar{\gamma}_{l,\epsilon} = 10$. The above parameters, Assumption 3, and Theorem 2 allow the controller gain matrix and N_{ji} as follows:

$$F_1 = \begin{bmatrix} -1.0110 & -0.0290 \\ -0.0890 & -0.7150 \end{bmatrix}, L_1 = \begin{bmatrix} 0.9032 & -0.5430 \\ 1.8169 & -1.4767 \end{bmatrix}, K_1 = \begin{bmatrix} -0.0471 & -0.0324 \\ 0.0168 & 0.0296 \end{bmatrix}, F_2 = \begin{bmatrix} -1.0120 & -0.037 \\ -0.0960 & -1.720 \end{bmatrix},$$

$$L_2 = \begin{bmatrix} -1.0629 & 0.4652 \\ 1.6772 & -0.3187 \end{bmatrix}, K_2 = \begin{bmatrix} -0.0510 & -0.3455 \\ 0.0471 & 0.3948 \end{bmatrix}, F_3 = \begin{bmatrix} -0.3200 & -0.1100 \\ -0.1200 & -0.4900 \end{bmatrix}, L_3 = \begin{bmatrix} -0.4064 & 0.2833 \\ 1.3492 & -0.2661 \end{bmatrix},$$

$$K_3 = \begin{bmatrix} 0.0137 & -0.0308 \\ 0.0190 & -0.0264 \end{bmatrix}, N_{12} = N_{21} = \begin{bmatrix} 0.0785 & -0.0222 & 0.0003 & 0.0002 \\ -0.0231 & 0.0681 & -0.0004 & -0.0005 \\ 0.0003 & -0.0013 & 0.0722 & -0.1014 \\ 0.0001 & -0.0005 & -0.0104 & 0.0714 \end{bmatrix},$$

$$N_{13} = N_{31} = \begin{bmatrix} -0.2992 & 0.0771 & -0.0014 & -0.0016 \\ 0.0795 & -0.2224 & 0.0016 & -0.0004 \\ -0.0015 & 0.0017 & -0.4929 & 0.0571 \\ -0.0015 & -0.0002 & 0.0586 & -0.3489 \end{bmatrix}, N_{23} = N_{32} = \begin{bmatrix} 0.4831 & -0.2821 & -0.2501 & -0.0936 \\ -0.0130 & 0.1489 & -0.1608 & -0.0484 \\ -0.04475 & -0.3751 & 0.6284 & -0.0502 \\ -0.0204 & -0.1629 & -0.1235 & 0.6543 \end{bmatrix}.$$

The trigger interval of METMs (3) is depicted in Figure 3 with the shaded portion being the attack intervals, where the switching-Q-learning algorithm trains the triggering thresholds in the second stage of METM. From the resilient switching rule in Figure 4, the pink dashed box marks the subsystem switching after its $\mathcal{T}_{\min}$ when there is no LDDoS attack; the red dashed box signifies that when an attack occurs from 1.6 to 2.1 s, the activation interval of the subsystem is 0.498 s. Figure 5 depicts the evolution of $V(t)$, including a purple dashed box indicating the absence of a monotonic reduction in $V(t)$, which

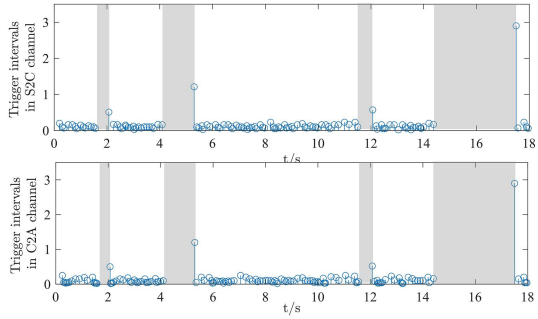

Figure 3 (Color online) Trigger intervals in dual networks and $\mathbb{H}_p^{\varsigma}$.

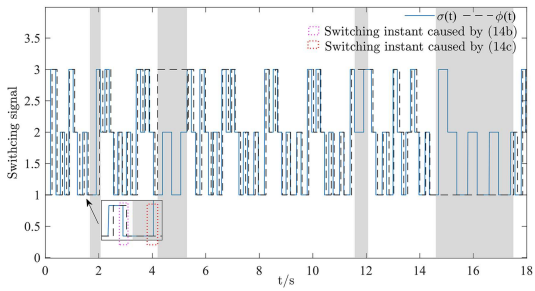

Figure 4 (Color online) Switching signals of $\sigma(t)$ and $\phi(t)$.

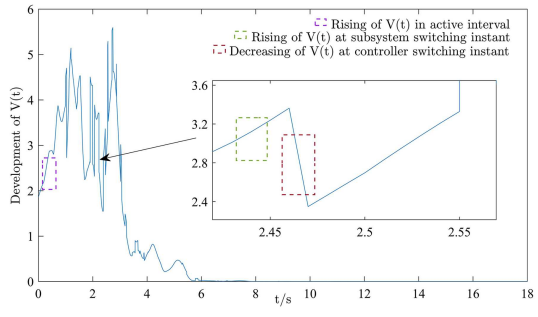

Figure 5 (Color online) Development of $V(t)$.

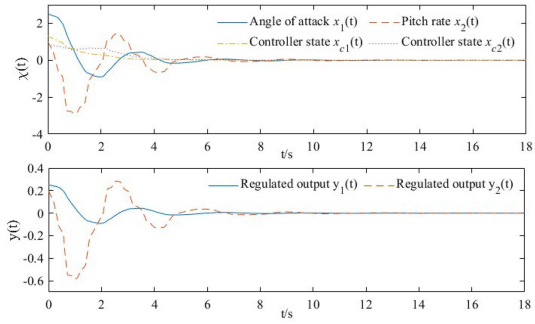

Figure 6 (Color online) State responses and regulated outputs of (13).

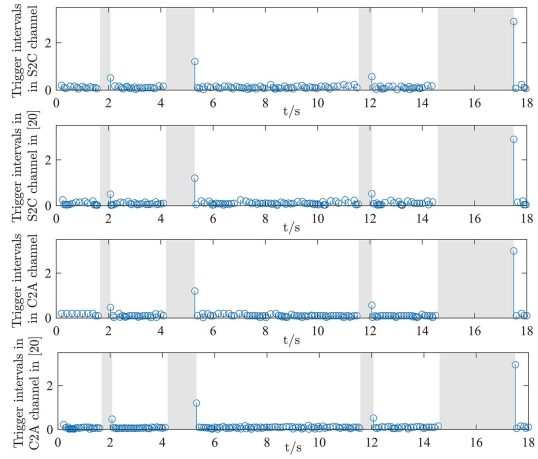

Figure 7 (Color online) Trigger intervals under METMs (3) and ETMs [20].

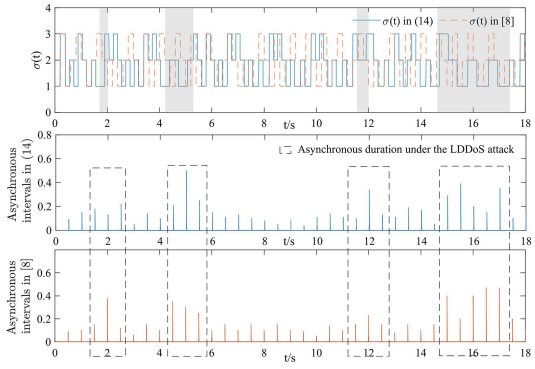

Figure 8 (Color online) $\sigma(t)$ and asynchronous durations in (14) and [8].

indicates the occurrence of the SUD. $V(t)$ at the subsystem switching instant 2.39 s, as indicated by the green dashed box in Figure 5, exhibits an increasing trend, whereas its value at the corresponding controller switching instant 2.46 s, denoted by the red dashed box, demonstrates a decreasing pattern. This observation suggests that the stability of ℓ_q is not correlated with $\tilde{\ell}_q$. Figure 6 reflects the state response and regulated outputs under the initial state $\mathcal{X}^{\mathrm{T}}(0) = [2.5\ 1\ 1.3\ 0.8]$.

The triggering interval and number are compared in Figure 7 and Table 1 between the ETM with a static threshold in [20], which means the threshold was not learned, and the METM (3) with optimal thresholds trained 50 times in switching-Q-learning. It is clear that Eq. (3) has superior performance. In examining the same LDDoS attack, a comparison is made in Figure 8 between the switching signals under

Table 1 Triggering number under different ETMs ($T = 18$ s)

ETMs	Triggering number in S2C channel	Triggering number in C2A channel
METM (3) under the switching-Q-learning	105	136
ETM without learning in [20]	134	163

Table 2 Asynchronous duration and switching under different switching rules ($T = 18$ s)

Switching rule	The asynchronous duration (s)	The number of asynchronous switching
Resilient switching rule (14)	6.32	12
DT switching rule [8]	6.60	23

the DT in [8] and (14). It is noticeable that the introduction of attack parameters $\mathbb{H}_p^y$ in (14a) and (14b) results in a lower switching number, particularly within the gray-shaded attack intervals. The asynchrony duration under (14) is observed to be shorter, as indicated by the black dashed box in Figure 8. Table 2 displays the asynchronous duration and switching corresponding to [8] and (14).

5 Conclusion

This paper tackles the SOR problem for NSSs with SUDs under LDDoS attacks by proposing a resilient switching rule that prolongs subsystem DT during LDDoS attacks to mitigate consecutive asynchronous durations. It establishes METMs that learn the optimal threshold using the switching-Q-learning algorithm to adjust data transmission in the network and shorten asynchronous durations. Finally, solvability conditions for permitted SOR under DOFC are derived. Future research may focus on developing active defense strategies for systems under attacks.

Acknowledgements This work was supported by National Natural Science Foundation of China (Grant Nos. 62273068, U23A203-24) and Natural Science Foundation of Liaoning Province (Grant No. 2023-MS-120).

References

1 Zhang W, Zeng J, Zhang J, et al. H_∞ consensus tracking of recovery system for multiple unmanned underwater vehicles with switching networks and disturbances. Ocean Eng, 2022, 245: 110589
2 Zhang Z X, Song H F, Wang H W, et al. A model predictive control strategy with switching cost functions for cooperative operation of trains. Sci China Inf Sci, 2023, 66: 172206
3 Zhao J, Yang C, Wang W, et al. A game-learning-based smooth path planning strategy for intelligent air-ground vehicle considering mode switching. IEEE Trans Transp Electrific, 2022, 8: 3349–3366
4 Qu H Q, Zhao J. Stabilisation of switched linear systems under denial of service. IET Control Theor & Appl, 2020, 14: 1438–1444
5 Han Y C, Lian J, Huang X. Event-triggered H_∞ control of networked switched systems subject to denial-of-service attacks. Nonlinear Anal-Hybrid Syst, 2020, 38: 100930
6 Wang Y W, Zeng Z H, Liu X K, et al. Input-to-state stability of switched linear systems with unstabilizable modes under DoS attacks. Automatica, 2022, 146: 110607
7 Zhao R, Zuo Z Q, Wang Y J. Event-triggered control for switched systems with denial-of-service attack. IEEE Trans Automat Contr, 2022, 67: 4077–4090
8 Li L L, Fu J, Zhang Y, et al. Mixed event-triggered output regulation for networked switched systems with unstable switching dynamics under long-duration DoS attacks. IEEE Trans Cybern, 2023, 53: 7150–7161
9 Hespanha J P, Morse A S. Stability of switched systems with average dwell-time. In: Proceedings of the 38th IEEE Conference on Decision and Control, 1999. 2655–2660
10 Zhang N K, Kang Y, Yu P L. Stability analysis of discrete-time switched positive nonlinear systems with unstable subsystems under different switching strategies. IEEE Trans Circuits Syst II, 2021, 68: 1957–1961
11 Ma R C, An S, Fu J. Dwell-time-based stabilization of switched positive systems with only unstable subsystems. Sci China Inf Sci, 2021, 64: 119205
12 Li L L, Zhang Y, Li T S. Memory-based event-triggered output regulation for networked switched systems with unstable switching dynamics. IEEE Trans Cybern, 2022, 52: 12429–12439
13 Branicky M S. Multiple Lyapunov functions and other analysis tools for switched and hybrid systems. IEEE Trans Automat Contr, 1998, 43: 475–482
14 Zhao J, Hill D J. On stability, L_2-gain and H_∞ control for switched systems. Automatica, 2008, 44: 1220–1232
15 Li L L, Zhao J, Dimirovski G M. Multiple Lyapunov functions approach to observer-based H_∞ control for switched systems. Int J Syst Sci, 2013, 44: 812–819
16 Allerhand L I, Shaked U. Robust state-dependent switching of linear systems with dwell time. IEEE Trans Automat Contr, 2013, 58: 994–1001
17 Sang H, Nie H. Asynchronous H_∞ control for discrete-time switched systems under state-dependent switching with dwell time constraint. Nonlinear Anal-Hybrid Syst, 2018, 29: 187–202
18 Zhang S Y, Nie H. Dwell-time-dependent asynchronous mixed H_∞ and passive control for discrete-time switched systems. Nonlinear Anal-Hybrid Syst, 2022, 44: 101140
19 Tabuada P. Event-triggered real-time scheduling of stabilizing control tasks. IEEE Trans Automat Contr, 2007, 52: 1680–1685

20 Li L L, Fu J, Zhang Y, et al. Output regulation for networked switched systems with alternate event-triggered control under transmission delays and packet losses. Automatica, 2021, 131: 109716
21 Cheng J, Xie L F, Zhang D, et al. Novel event-triggered protocol to sliding mode control for singular semi-Markov jump systems. Automatica, 2023, 151: 110906
22 Cao L, Pan Y N, Liang H J, et al. Observer-based dynamic event-triggered control for multiagent systems with time-varying delay. IEEE Trans Cybern, 2023, 53: 3376–3387
23 Ma H, Li H Y, Lu R Q, et al. Adaptive event-triggered control for a class of nonlinear systems with periodic disturbances. Sci China Inf Sci, 2020, 63: 150212
24 Xie X H, Hu S L, Liu Y G, et al. Resilient adaptive event-triggered H_∞ fuzzy filtering for cyber-physical systems under stochastic-sampling and denial-of-service attacks. IEEE Trans Fuzzy Syst, 2023, 31: 278–292
25 Zhang D, Ye Z H, Feng G, et al. Intelligent event-based fuzzy dynamic positioning control of nonlinear unmanned marine vehicles under DoS attack. IEEE Trans Cybern, 2022, 52: 13486–13499
26 Ye Z H, Zhang D, Wu Z G, et al. A3C-based intelligent event-triggering control of networked nonlinear unmanned marine vehicles subject to hybrid attacks. IEEE Trans Intell Transp Syst, 2022, 23: 12921–12934
27 Lu J W, Han L Y, Wei Q L, et al. Event-triggered deep reinforcement learning using parallel control: a case study in autonomous driving. IEEE Trans Intell Veh, 2023, 8: 2821–2831
28 Ren H L, Zong G D, Shi K B. Event-triggered finite-time H_∞ output tracking control of switched systems with round-robin protocol and its applications. Intl J Robust Nonlinear, 2021, 31: 6123–6143
29 Hu S L, Yue D, Chen X L, et al. Resilient H_∞ filtering for event-triggered networked systems under nonperiodic DoS jamming attacks. IEEE Trans Syst Man Cybern Syst, 2021, 51: 1392–1403
30 Li T F, Fu J, Niu B. Hysteresis-based switching design for stabilization of switched linear neutral systems. Circuits Syst Signal Process, 2017, 36: 359–373
31 Park P G, Ko J W, Jeong C. Reciprocally convex approach to stability of systems with time-varying delays. Automatica, 2011, 47: 235–238
32 Fridman E. Output regulation of nonlinear systems with delay. Syst Control Lett, 2003, 50: 81–93
33 Xiong J, Lam J. Stabilization of networked control systems with a logic ZOH. IEEE Trans Automat Contr, 2009, 54: 358–363
34 Adams R J, Buffington J M, Sparks A G, et al. Robust Multivariable Flight Control. London: Springer, 1994. 45–95